J. Fluid Mech. (1995), *vol.* 305, *pp.* 185–218

Compressible turbulent channel flows: DNS results and modelling

By P. G. HUANG[1]†, G. N. COLEMAN[2] AND P. BRADSHAW[3]

[1]MCAT, Inc. San Jose, CA 95127, USA

[2]Mechanical, Aerospace, and Nuclear Engineering Department, Univ. of California, Los Angeles, CA 90024-1597, USA

[3]Department of Mechanical Engineering, Stanford University, Stanford, CA 94305-3030, USA

(Received 1 November 1994 and in revised form 11 August 1995)

The present paper addresses some topical issues in modelling compressible turbulent shear flows. The work is based on direct numerical simulation (DNS) of two supersonic fully developed channel flows between very cold isothermal walls. Detailed decomposition and analysis of terms appearing in the mean momentum and energy equations are presented. The simulation results are used to provide insights into differences between conventional Reynolds and Favre averaging of the mean-flow and turbulent quantities. Study of the turbulence energy budget for the two cases shows that compressibility effects due to turbulent density and pressure fluctuations are insignificant. In particular, the dilatational dissipation and the mean product of the pressure and dilatation fluctuations are very small, contrary to the results of simulations for sheared homogeneous compressible turbulence and to recent proposals for models for general compressible turbulent flows. This provides a possible explanation of why the Van Driest density-weighted transformation (which ignores any true turbulent compressibility effects) is so successful in correlating compressible boundary-layer data. Finally, it is found that the DNS data do not support the strong Reynolds analogy. A more general representation of the analogy is analysed and shown to match the DNS data very well.

1. Introduction

There has been considerable evidence that the Van Driest density-weighted transformation (see Van Driest 1951) can collapse velocity profiles of compressible turbulent boundary layers onto the incompressible law of the wall (see for example Fernholz & Finley 1980; Huang, Bradshaw & Coakley 1993; Huang & Coleman 1994). Since the Van Driest transformation can be viewed as a straightforward extension of the mixing-length model, the implication is that the difference between compressible and incompressible turbulent boundary layers is mainly due to *mean* density variations, while compressibility effects resulting from turbulent density and pressure fluctuations are negligible. This proposition is in line with the Morkovin hypothesis (see Morkovin 1964), which postulates that the essential dynamics of compressible turbulent boundary layers closely follow the incompressible pattern, as long as the r.m.s. fluctuating Mach number is small (as in a boundary layer with free-stream Mach number less than 5, say).

† Mailing address: mail stop 229-1, NASA Ames Research Center, Moffett Field, CA 94035, USA.

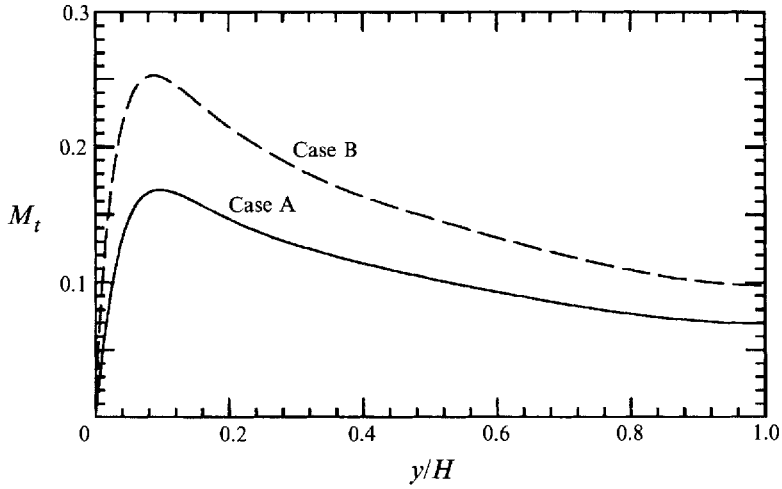

FIGURE 1. Turbulent Mach number in a fully developed compressible channel flow – Case A: $(Re, M, \langle T_c\rangle/T_w) = (3000, 1.5, 1.38)$ and Case B: $(Re, M, \langle T_c\rangle/T_w) = (4880, 3, 2.47)$.

Recent work by Huang *et al.* (1993) has shown that the Van Driest transformation can also be applied in hypersonic regions (up to Mach 11) as well as in non-adiabatic situations. Furthermore, in the recently completed study by Huang & Coleman (1994) using data from a compressible channel flow direct numerical simulation (DNS) of Coleman *et al.* (1993) and Coleman, Kim & Moser (1995), the companion paper to this, it was found that a simple 'variable-mean-density' extension of the mixing length model is adequate to represent the compressible law of the wall, although the turbulent Mach number†, $M_t \equiv \langle k\rangle^{1/2}/\langle a\rangle$, of the DNS data, as depicted in figure 1, is about the same as in a compressible turbulent mixing layer at a convective Mach number of 1. (In the above, $\langle k\rangle \equiv \langle u_i'u_i'\rangle/2$ is the ensemble-averaged turbulent kinetic energy per unit mass, and $\langle a\rangle$ is the mean speed of sound; see §2 for further definitions.) These studies have suggested that compressibility effects due to turbulent fluctuations may not be as strong at a given M_t in boundary layers as in mixing layers (cf. Sarkar 1995).

In this study we again consider results from the DNS of Coleman *et al.* (1993, 1995), which are of fully developed supersonic flow in a channel with cooled walls, with constant specific heats, $\gamma = c_p/c_v = 1.4$ and a constant Prandtl number of 0.7. As explained in §3, the flow is driven by a constant body force per unit mass rather than a constant pressure gradient: because the density varies across the channel, so does the equivalent pressure gradient, but this does not affect our qualitative conclusions. The DNS solutions include two cases: A, with Reynolds number $Re = 3000$, Mach number $M = 1.5$ and mean channel centreline-to-wall temperature ratio $\langle T_c\rangle/T_w = 1.38$; and B, with $Re = 4880$, $M = 3$ and $\langle T_c\rangle/T_w = 2.47$. Here Re is based on the bulk density, $\rho_m \equiv \int_0^H \langle\rho\rangle \mathrm{d}y/H$, bulk velocity, $U_m \equiv \dot{m}/\rho_m$ (where $\dot{m} \equiv \int_0^H \langle\rho u\rangle \mathrm{d}y/H$ is the mass flow rate per unit area), channel half-width, H, and wall viscosity, μ_w; and M on the bulk velocity and wall sound speed, a_w (the subscript w is used throughout to denote the value at the wall). In addition, the data presented by Kim, Moin & Moser (1987) and Mansour, Kim & Moin (1988) for an incompressible channel flow with $Re = 2790$ are shown for purpose of comparison. Coleman *et al.* (1995) attempted to

† Some other workers have used different definitions, e.g. $M_t \equiv (2\langle k\rangle)^{1/2}/\langle a\rangle$. The present choice is most convenient for discussion of models.

	Incompressible†	Compressible‡	
		Case A	Case B
Re	2790	3000	4880
M	0	1.5	3
$\langle T_c\rangle/T_w$	1	1.38	2.49
$\langle\rho_c\rangle\langle u_c\rangle H/\langle\mu_c\rangle$	3250	2760	2871
$H^* \equiv H\langle\rho_c\rangle(\tau_w/\langle\rho_c\rangle)^{1/2}/\langle\mu_c\rangle$	180	151	150
u_τ/U_m	0.0645	0.0545	0.0387
maximum M_t	0	0.168	0.253

† Kim *et al.* (1987)

‡ Coleman *et al.* (1995)

TABLE 1. Comparison of the channel flow DNS (Re and M are based on the bulk velocity, the bulk density, and the viscosity and the sound speed at the wall).

minimize differences due to Reynolds number effects by making the local Reynolds numbers, $\langle\rho\rangle\langle u\rangle y/\langle\mu\rangle$ (where $\langle\rho\rangle$, $\langle u\rangle$ and $\langle\mu\rangle$ are the local mean density, velocity and viscosity, respectively), of the three cases as similar as possible. A comparison of conditions used in the three channel flow DNS is presented in table 1 (see also table 3 of Coleman *et al.* 1995). The centreline Reynolds numbers $\langle\rho_c\rangle\langle u_c\rangle H/\langle\mu_c\rangle$ are 3250, 2760 and 2871 for the incompressible DNS and for compressible Cases A and B, respectively; the corresponding values of y^* ($\equiv \langle\rho\rangle y(\tau_w/\langle\rho\rangle)^{1/2}/\langle\mu\rangle$) at the centre of the channel ($y = H$) are 180, 151 and 150. Furthermore, as will be seen below, the budgets of the mean momentum, energy and turbulent kinetic energy equations for the three cases are very similar – indicating that discrepancies resulting from Reynolds number effects are indeed small. These data offer a unique opportunity: (i) to compare conventional Reynolds or ensemble averaging (commonly referred to as 'time' averaging; in the current stationary DNS this is done by averaging over time and planes parallel to the walls) and mass-weighted averaging (commonly referred to as 'Favre' averaging, although Reynolds (1895) was the first to propose it); (ii) to investigate transfer between the mean, turbulcnt and internal energies; (iii) to study the influence of terms containing density fluctuations; (iv) to assess compressibility contributions due to turbulent fluctuations in the overall energy budget; and (v) to validate the concept of the strong Reynolds analogy and its variants.

In this paper, all results will be plotted against y/H. To obtain the corresponding wall coordinate, $y^+ = \rho_w y u_\tau/\mu_w$ (where $u_\tau = (\tau_w/\rho_w)^{1/2}$, with $\rho_w \equiv \langle\rho_w\rangle$), for the incompressible case and compressible Cases A and B, one should multiply y/H by 180, 222 and 451, respectively. The incompressible DNS shows that at the beginning of the fully turbulent region, $y^+ \approx 30$ say, the value of $\langle\tau_{12}\rangle/\langle\tau_T\rangle$ (where $\langle\tau_{12}\rangle$ and $\langle\tau_T\rangle$ denote mean viscous and total shear stress) is approximately 0.13. The corresponding y^* at $\langle\tau_{12}\rangle/\langle\tau_T\rangle = 0.13$ is approximately 31 and 30 for Cases A and B, respectively. The values of y/H at this position for the incompressible DNS and for Cases A and B are approximately 0.17, 0.2 and 0.19, respectively. Comparisons of y^+ *vs.* y^* and y/H *vs.* y^* for the three cases are presented in figure 2. The lines for incompressible flow are exactly straight; those for compressible flow are nearly straight because the temperature is nearly constant except near the wall (see figure 4). Although there is no unique definition of y^+ that will collapse all compressible channel flow data, we find that y^* (which is based on τ_w and local properties) is perhaps the best among three possible definitions for the wall coordinate: $\rho_w y u_\tau/\mu_w$, $\rho y u_\tau/\mu$ and $\rho(\tau_w/\rho)^{1/2} y/\mu$.

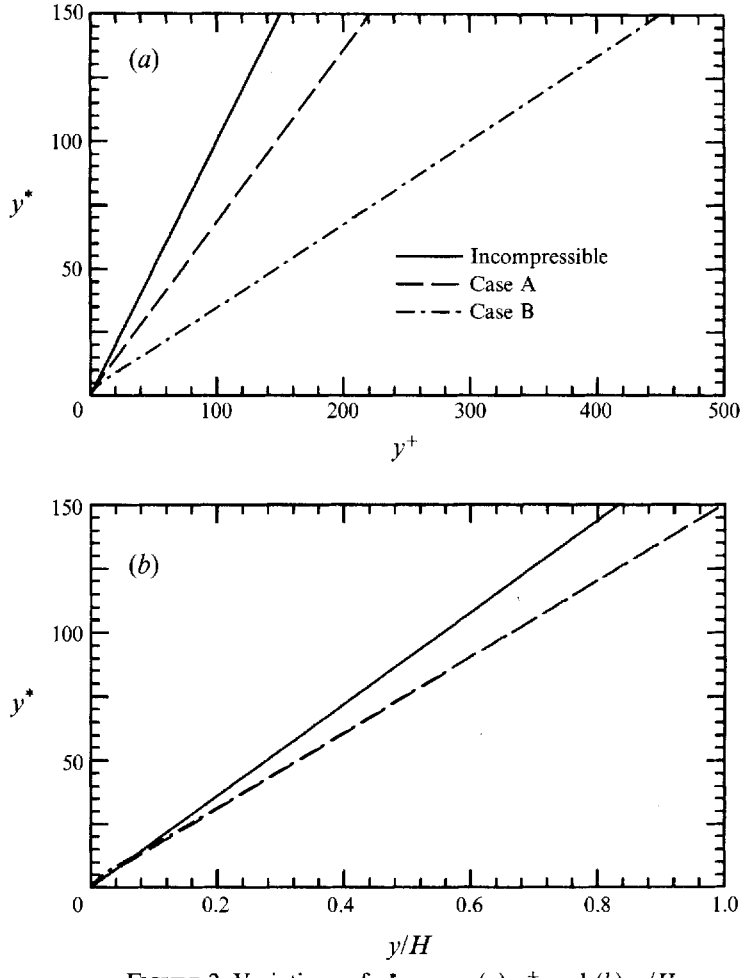

FIGURE 2. Variations of y^* versus (*a*) y^+ and (*b*) y/H.

2. Reynolds and Favre averaging

First, let us define the following: $\langle\ \rangle$ the ensemble average and $\{\ \}$ the Favre average given by $\{f\} = \langle\rho f\rangle/\langle\rho\rangle$; the single prime, $'$, and the double prime, $''$, represent the turbulent fluctuations with respect to Reynolds and Favre averages, respectively. The dependent variables are decomposed according to:

$$\left.\begin{aligned} \rho' &= \rho - \langle\rho\rangle, \\ u_i'' &= u_i - \{u_i\}, \\ T'' &= T - \{T\}, \\ \langle p\rangle &= \langle\rho\rangle R\{T\} = \langle\rho\rangle R\langle T\rangle + R\langle\rho' T'\rangle, \\ &= \langle\rho\rangle R(\langle T\rangle - \langle T''\rangle), \\ p' &= \rho' R\{T\} + \langle\rho\rangle R T'' + R\rho' T'', \\ \{u_i'' u_j''\} &= \langle\rho u_i'' u_j''\rangle/\langle\rho\rangle. \end{aligned}\right\} \tag{2.1}$$

It should be noted that $\langle f'\rangle = 0$ and $\langle\rho f''\rangle = 0$ but $\langle f''\rangle \neq 0$.

The relationship between the Reynolds- and Favre-averaged quantities for velocities

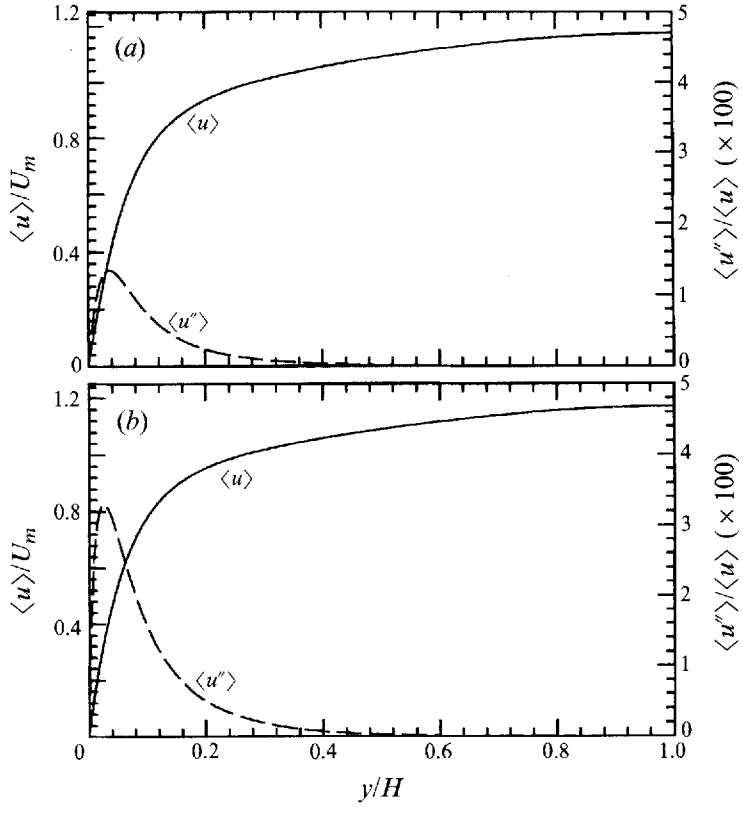

FIGURE 3. Streamwise velocity profiles – mean and fluctuating components: (*a*) Case A, (*b*) Case B.

and temperature can be written as

$$\langle f \rangle - \{f\} = \langle f'' \rangle = -\frac{\langle \rho' f' \rangle}{\langle \rho \rangle} = -\frac{\langle \rho' f'' \rangle}{\langle \rho \rangle}, \tag{2.2}$$

where $f \equiv u_i$ or T. Figures 3 and 4 compare the Reynolds-averaged mean streamwise velocity, $\langle u \rangle$, and its fluctuating component, $\langle u'' \rangle$, and the Reynolds-averaged mean temperature, $\langle T \rangle$, and its fluctuating component, $\langle T'' \rangle$, respectively. As can be seen from the figures, $\langle f \rangle \gg \langle f'' \rangle$ and the difference between Reynolds- and Favre-averaged quantities is mainly observed in the near-wall region ($y^* < 30$; i.e. $y/H < 0.2$ approximately) – the maximum $\langle u'' \rangle$ is about 3% of $\langle u \rangle$ for Case B, while the maximum $\langle T'' \rangle / \langle T \rangle$ is about 1.2%. Although $\langle f \rangle \approx \{f\}$, the slight variation of $\langle f'' \rangle$ causes some small differences between $\partial \langle f \rangle / \partial y$ and $\partial \{f\} / \partial y$ near the wall. We shall come back to this point later.

Relationships between the Reynolds- and Favre-averaged values for stresses and heat fluxes, respectively, can be written as

$$\{u_i'' u_j''\} = \langle u_i' u_j' \rangle - \langle u_i'' \rangle \langle u_j'' \rangle + \langle \rho' u_i' u_j' \rangle / \langle \rho \rangle, \tag{2.3}$$

$$\{u_i'' T''\} = \langle u_i' T' \rangle - \langle u_i'' \rangle \langle T'' \rangle + \langle \rho' u_i' T' \rangle / \langle \rho \rangle. \tag{2.4}$$

Figures 5 and 6 compare, respectively, the Reynolds- and Favre-averaged turbulent shear stresses and heat fluxes. The figures show that the terms associated with the products of the two mean Favre-averaged fluctuations, $\langle u'' \rangle \langle v'' \rangle$ and $\langle v'' \rangle \langle T'' \rangle$, are less than 1% and are confined to the sublayer region ($y/H < 0.1$, $y^* < 17$); thus they

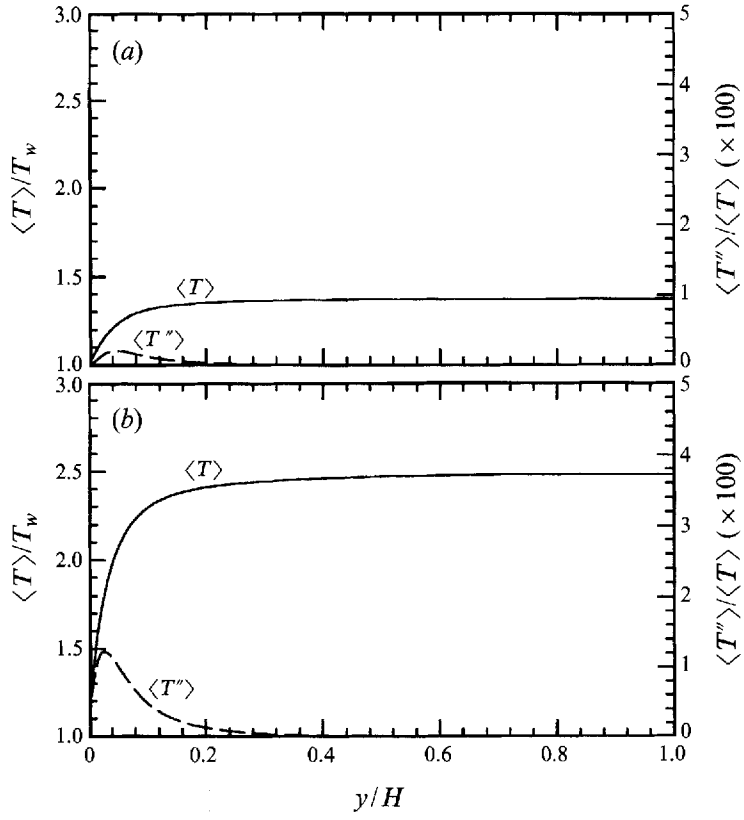

FIGURE 4. Temperature profiles – mean and fluctuating components: (*a*) Case A, (*b*) Case B.

can be neglected in general. The influence of the terms associated with the product of the triple Reynolds-averaged fluctuations, $\langle\rho' u' v'\rangle$ and $\langle\rho' v' T'\rangle$, extends outside the sublayer region, and $\langle\rho' u' v'\rangle$ and $\langle\rho' v' T'\rangle$ are at least one order of magnitude larger than $\langle\rho\rangle\langle u''\rangle\langle v''\rangle$ and $\langle\rho\rangle\langle v''\rangle\langle T''\rangle$, respectively. Thus, one can assume

$$\langle\rho u'' v''\rangle \approx \langle\rho u' v'\rangle = \langle\rho\rangle\langle u' v'\rangle + \langle\rho' u' v'\rangle, \tag{2.5}$$

$$\langle\rho v'' T''\rangle \approx \langle\rho v' T'\rangle = \langle\rho\rangle\langle v' T'\rangle + \langle\rho' v' T'\rangle. \tag{2.6}$$

Figure 7(*a–c*) compares distributions of the turbulent shear stress, $\{u''v''\}$, the turbulent kinetic energy, $\{k\} = \{u_i''^2\}/2$, and the turbulent heat flux, $\{v''T''\}$, respectively. It can be seen that, when normalized by $u_\tau = (\tau_w/\rho_w)^{1/2}$ and $T_\tau = q_w/\rho_w c_p u_\tau$, the profiles show a strong sensitivity to Mach number. On the other hand, if the density scale $\langle\rho\rangle/\rho_w$ is taken into account, as suggested by Morkovin (1964) and later by Spina, Smits & Robinson (1994), the data fall much closer to the corresponding incompressible curves (since there are inevitable Reynolds number differences between the three cases, as explained in the introduction, the data would not collapse exactly even if there were no compressibility effects). Although the need for this 'density transformation' may be obvious to many (since, outside the sublayer, $\langle\tau_t\rangle/\tau_w \equiv -\langle\rho\rangle\{u''v''\}/(\rho_w u_\tau^2) \approx 1-y/H$ and $\langle q_t\rangle/q_w \equiv -\langle\rho\rangle(\{u\}\{u''v''\}+\{v''u_i''u_i''\}/2+c_p\{v''T''\})/(\rho_w u_\tau c_p T_\tau) \approx 1-y/H$ almost independent of Mach number), the good collapse reaffirms the assumption that for supersonic flows the major effect of Mach number is due to mean density variations.

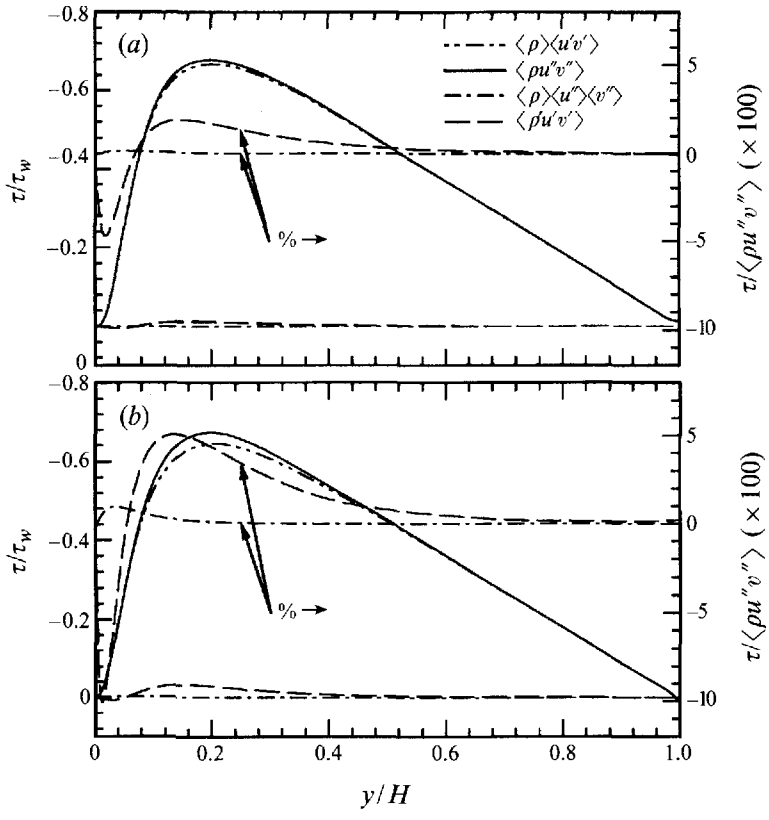

FIGURE 5. Decomposition of the Favre-averaged turbulent shear stress profiles. Symbol τ denotes any contribution to shear stress. (*a*) Case A, (*b*) Case B.

The decomposition of $u_i^2/2$, which may be called the 'instantaneous (total) kinetic energy', is less straightforward. Substituting the Favre mean and fluctuating velocities, one obtains

$$\tfrac{1}{2}u_iu_i = \tfrac{1}{2}\{u_i\}\{u_i\} + \{u_i\}u_i'' + \tfrac{1}{2}u_i''u_i''. \tag{2.7}$$

The first term on the right-hand side of equation (2.7) is the Favre-averaged mean-flow kinetic energy, $\{K\} = \{u_i\}^2/2$; the second term is $K'' = \{u_i\}u_i''$, which satisfies $\langle\rho K''\rangle = 0$ and may be called the 'Favre-fluctuating mean-flow kinetic energy', a choice justified when one examines the Favre-averaged total energy equation: the term associated with the turbulent diffusion of $\{K\}$ is $\partial(\langle\rho\rangle\{u_i\}\{u_i''u_k''\})/\partial x_k \equiv \partial(\langle\rho\rangle\{u_k''K''\})/\partial x_k$, showing that this definition of K'' has a physical interpretation. Since the Favre-averaged turbulent kinetic energy is $\{k\} = \{u_i''^2\}/2$, the Favre-fluctuating turbulent kinetic energy becomes $k'' = u_i''^2/2 - \{u_i''^2\}/2$ and it also satisfies $\langle\rho k''\rangle = 0$. Similarly, one may define the Reynolds-averaged mean-flow kinetic energy as $\langle K\rangle = \langle u_i\rangle^2/2$, the Reynolds-fluctuating mean-flow kinetic energy as $K' = \langle u_i\rangle u_i'$, the Reynolds-averaged turbulent kinetic energy as $\langle k\rangle = \langle u_i'^2\rangle/2$, and the Reynolds-fluctuating turbulent kinetic energy $k' = u_i'^2/2 - \langle u_i'^2\rangle/2$. Both $\langle K'\rangle$ and $\langle k'\rangle$ are zero by definition.

By definition one can also show that

$$\{K\} + \{k\} + K'' + k'' = \langle K\rangle + \langle k\rangle + K' + k', \tag{2.8}$$

$$\langle K\rangle + K' = \{K\} + K'' - \tfrac{1}{2}\langle u_i''\rangle^2 + \langle u_i''\rangle u_i'', \tag{2.9}$$

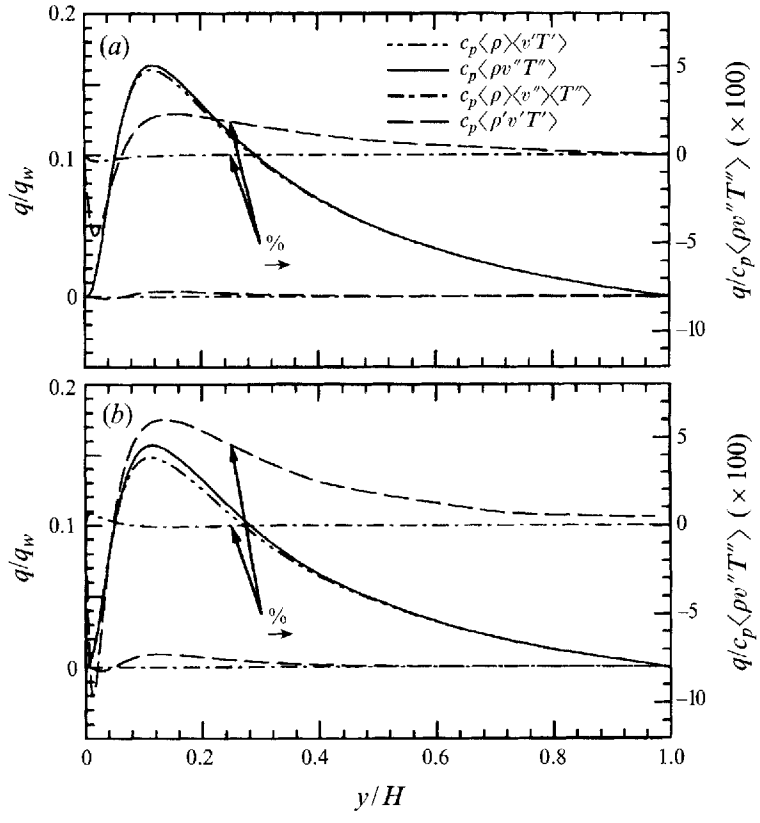

FIGURE 6. Decomposition of the Favre-averaged turbulent heat flux profiles. Symbol q denotes any contribution to heat flux. (*a*) Case A, (*b*) Case B.

$$\langle k\rangle + k' = \{k\} + k'' + \tfrac{1}{2}\langle u_i''\rangle^2 - \langle u_i''\rangle u_i'', \tag{2.10}$$

and therefore

$$\{K\} + \{k\} + \langle K''\rangle + \langle k''\rangle = \langle K\rangle + \langle k\rangle, \tag{2.11}$$

$$\langle K\rangle = \{K\} + \langle K''\rangle + \tfrac{1}{2}\langle u_i''\rangle^2, \tag{2.12}$$

$$\langle k\rangle = \{k\} + \langle k''\rangle - \tfrac{1}{2}\langle u_i''\rangle^2. \tag{2.13}$$

Equation (2.13) can also be derived directly from equation (2.3). Equations (2.11) to (2.13) illustrate that the 'mean/turbulent' partitions of the Favre and Reynolds averages are different even though their sum is the same. Furthermore, by ensemble averaging K'' and k'', one finds

$$\langle K''\rangle = \{u_i\}\langle u_i''\rangle, \tag{2.14}$$

$$\langle k''\rangle = \tfrac{1}{2}\langle u_i''u_i''\rangle - \tfrac{1}{2}\{u_i''u_i''\}. \tag{2.15}$$

The evaluation of $\langle K''\rangle$ is straightforward, but that of $\langle k''\rangle$ is not, because the first term on the right-hand side of (2.15) is the Reynolds-averaged value of $u_i''u_i''$, not the Favre-averaged value. However, it can be can shown that

$$\langle u_i''u_i''\rangle = \langle u_i'u_i'\rangle + \langle u_i''\rangle^2. \tag{2.16}$$

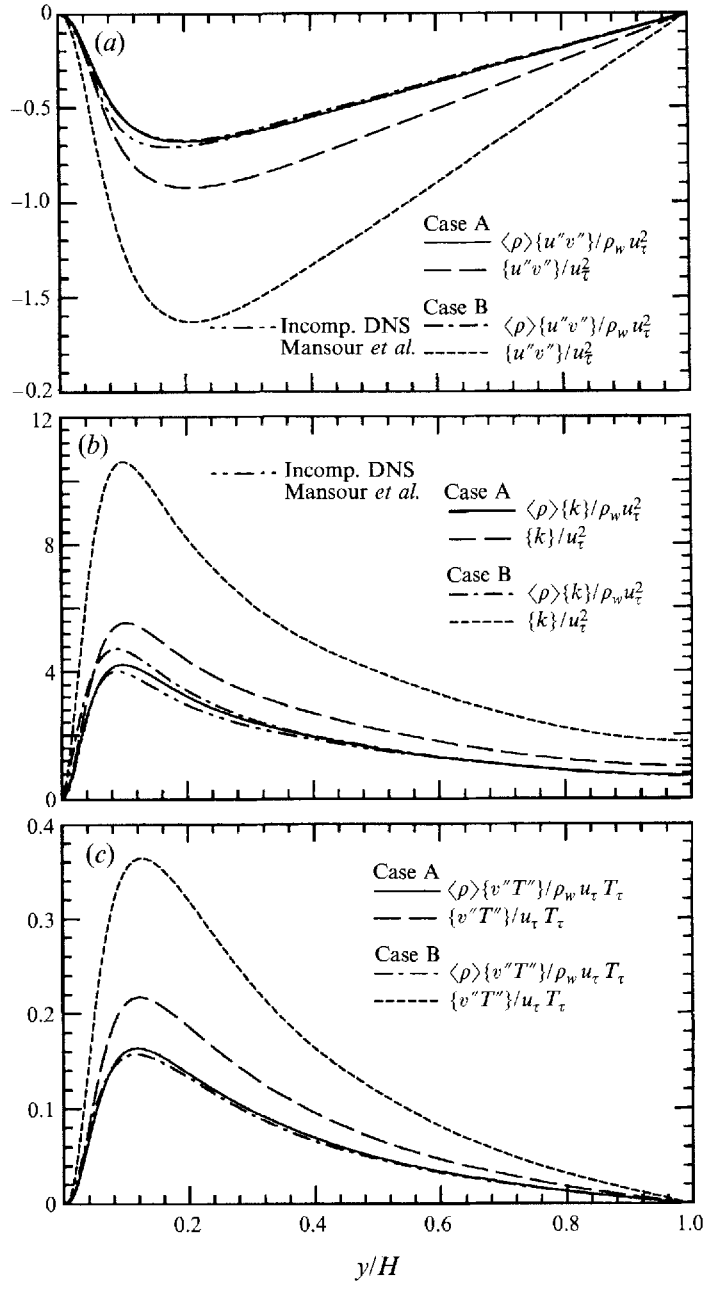

FIGURE 7. The effect of density scaling: (*a*) turbulent shear stress, (*b*) turbulent kinetic energy and (*c*) turbulent heat flux.

Hence, by substituting (2.3) and (2.16) into (2.15), one finds that

$$\langle k''\rangle = \langle u_i''\rangle^2 - \frac{1}{2}\frac{\langle \rho' u_i' u_i'\rangle}{\langle\rho\rangle}. \tag{2.17}$$

We evaluated $\langle k''\rangle$ using both (2.15) and (2.17), and found that the difference is less than 0.5% in the region where $\langle k''\rangle$ is not nearly zero ($0 < y/H < 0.5$). The

small difference is due to incomplete convergence of the ensemble averages in the simulations.

The decomposition of molecular stresses and heat fluxes, τ_{ij} and q_k, also requires some care. The Favre-averaging decomposition is only useful in handling the convective terms, since density appears explicitly in the formulation of convective fluxes; it is less advantageous for the molecular diffusive components, since it gives rise to additional terms such as $\partial\langle\tau_{ik}''\rangle/\partial x_k$. It is unlikely that any averaging system can be formed that completely eliminates density variations from the equations. To avoid dealing with terms like $\langle\tau_{ik}''\rangle$ in the mean momentum equation, one can first apply the Reynolds-averaging decomposition to the molecular stresses (or heat fluxes) and then replace the Reynolds-averaged dependent variables by the Favre-averaged ones using relationships such as (2.2), (2.12) and (2.13). The additional ensemble-averaged Favre fluctuating quantities, for example $\langle u_i''\rangle$, $\langle T''\rangle$, $\langle K''\rangle$ and $\langle k''\rangle$, are extra unknowns appearing in the mean-flow equations. They will be discussed further in the next section.

By substituting the Reynolds-averaged mean and fluctuating velocities and temperature into the definitions of τ_{ij} and q_k, one finds

$$\tau_{ik} = \left[\langle\mu\rangle\left(\frac{\partial\langle u_i\rangle}{\partial x_k}+\frac{\partial\langle u_k\rangle}{\partial x_i}\right)-\frac{2}{3}\langle\mu\rangle\frac{\partial\langle u_l\rangle}{\partial x_l}\delta_{ik}\right]+\left[\langle\mu\rangle\left(\frac{\partial u_i'}{\partial x_k}+\frac{\partial u_k'}{\partial x_i}\right)-\frac{2}{3}\langle\mu\rangle\frac{\partial u_l'}{\partial x_l}\delta_{ik}\right]$$
$$+\left[\mu'\left(\frac{\partial u_i'}{\partial x_k}+\frac{\partial u_k'}{\partial x_i}\right)-\frac{2}{3}\mu'\frac{\partial u_l'}{\partial x_l}\delta_{ik}\right]+\left[\mu'\left(\frac{\partial\langle u_i\rangle}{\partial x_k}+\frac{\partial\langle u_k\rangle}{\partial x_i}\right)-\frac{2}{3}\mu'\frac{\partial\langle u_l\rangle}{\partial x_l}\delta_{ik}\right] \quad (2.18)$$

and

$$q_k = -\langle\alpha\rangle\frac{\partial\langle T\rangle}{\partial x_k}-\alpha'\frac{\partial\langle T\rangle}{\partial x_k}-\langle\alpha\rangle\frac{\partial T'}{\partial x_k}-\alpha'\frac{\partial T'}{\partial x_k} \quad (2.19)$$

where α is the thermal conductivity. For future reference, we define

$$\langle\tau_{ik}\rangle = \left[\langle\mu\rangle\left(\frac{\partial\langle u_i\rangle}{\partial x_k}+\frac{\partial\langle u_k\rangle}{\partial x_i}\right)-\frac{2}{3}\langle\mu\rangle\frac{\partial\langle u_l\rangle}{\partial x_l}\delta_{ik}\right]$$
$$+\left[\left\langle\mu'\left(\frac{\partial u_i'}{\partial x_k}+\frac{\partial u_k'}{\partial x_i}\right)\right\rangle-\frac{2}{3}\left\langle\mu'\frac{\partial u_l'}{\partial x_l}\right\rangle\delta_{ik}\right], \quad (2.20)$$

$$\tau_{ik}' = \left[\mu'\left(\frac{\partial u_i'}{\partial x_k}+\frac{\partial u_k'}{\partial x_i}\right)-\frac{2}{3}\mu'\frac{\partial u_l'}{\partial x_l}\delta_{ik}\right]-\left[\left\langle\mu'\left(\frac{\partial u_i'}{\partial x_k}+\frac{\partial u_k'}{\partial x_i}\right)\right\rangle-\frac{2}{3}\left\langle\mu'\frac{\partial u_l'}{\partial x_l}\right\rangle\delta_{ik}\right]$$
$$+\left[\langle\mu\rangle\left(\frac{\partial u_i'}{\partial x_k}+\frac{\partial u_k'}{\partial x_i}\right)-\frac{2}{3}\langle\mu\rangle\frac{\partial u_l'}{\partial x_l}\delta_{ik}\right]+\left[\mu'\left(\frac{\partial\langle u_i\rangle}{\partial x_k}+\frac{\partial\langle u_k\rangle}{\partial x_i}\right)-\frac{2}{3}\mu'\frac{\partial\langle u_l\rangle}{\partial x_l}\delta_{ik}\right] \quad (2.21)$$

and

$$\langle q_k\rangle = -\langle\alpha\rangle\frac{\partial\langle T\rangle}{\partial x_k}-\left\langle\alpha'\frac{\partial T'}{\partial x_k}\right\rangle, \quad (2.22)$$

$$q_k' = -\alpha'\frac{\partial T'}{\partial x_k}+\left\langle\alpha'\frac{\partial T'}{\partial x_k}\right\rangle-\alpha'\frac{\partial\langle T\rangle}{\partial x_k}-\langle\alpha\rangle\frac{\partial T'}{\partial x_k}. \quad (2.23)$$

The inclusion of correlations between the fluctuating viscosity (or fluctuating conductivity) and fluctuating rate of strain (or fluctuating temperature gradient) in the above is necessary in order to satisfy $\langle\tau_{ij}'\rangle = 0$ and $\langle q_k'\rangle = 0$.

3. Governing transport equations

To simplify the governing transport equations, the Favre decomposition is applied to the convective terms so that they can be reduced to exactly the same form as those obtained when the incompressible governing equations are averaged. For the rest of the terms, the Reynolds-averaged decomposition is applied since there is no advantage in using the Favre decomposition. The final equations contain a mix of Reynolds-averaged and Favre-averaged mean quantities. It should be noted that most CFD prediction methods further simplify the equations by replacing the Reynolds-averaged quantities by Favre averages, which may be justifiable because convection is probably the most significant mechanism in most turbulent flows. In this paper, however, we do not need to make such a simplification, since formulae derived in §2 concerning the relationships between the Favre- and Reynolds-averaged variables, (2.2), (2.12) and (2.13), can be used to write the final form of the equations in terms of only one set of variables – Reynolds averaged or Favre averaged. In the present discussion, we use equations based on the Favre decomposition.

Combining the expressions for the Favre-averaged and fluctuating quantities given in the previous section with the Navier–Stokes equations and averaging, the conservation equations become

$$\frac{\partial \langle\rho\rangle\{u_k\}}{\partial x_k} = 0, \tag{3.1}$$

$$\frac{\partial \langle\rho\rangle\{u_i\}\{u_k\}}{\partial x_k} + \frac{\partial \langle p\rangle}{\partial x_i} = \frac{\partial \langle\tau_{ik}\rangle}{\partial x_k} - \frac{\partial \langle\rho\rangle\{u_i''u_k''\}}{\partial x_k}, \tag{3.2}$$

$$\begin{aligned}\frac{\partial}{\partial x_k}\langle\rho\rangle\{u_k\}\left[(\{e\} + \langle p\rangle/\langle\rho\rangle) + \{K\} + \{k\}\right] &= \frac{\partial}{\partial x_k}\left(\langle\tau_{ik}\rangle\langle u_i\rangle + \langle\tau_{ik}'u_i'\rangle - \langle q_k\rangle\right) \\ &\quad - \frac{\partial}{\partial x_k}\left(\langle\rho\rangle\{u_k''K''\} + \langle\rho\rangle\{u_k''k''\} + \langle\rho\rangle c_p\{u_k''T''\}\right),\end{aligned} \tag{3.3}$$

where $\{e\} = c_v\{T\}$ is the internal energy. The molecular and turbulent diffusion terms are the first and second, respectively, on the right-hand side of both (3.2) and (3.3). Equation (3.3) represents the conservation of total energy: the sum of the internal, mean kinetic and turbulent kinetic energies. The turbulent kinetic energy equation is

$$\begin{aligned}\frac{\partial \langle\rho\rangle\{u_k\}\{k\}}{\partial x_k} &= -\langle\rho\rangle\{u_i''u_k''\}\frac{\partial\{u_i\}}{\partial x_k} - \frac{\partial \langle\rho\rangle\{u_k''k''\}}{\partial x_k} - \frac{\partial\langle p'u_k'\rangle}{\partial x_k} \\ &\quad + \frac{\partial\langle\tau_{ik}'u_i'\rangle}{\partial x_k} - \left\langle\tau_{ik}'\frac{\partial u_i'}{\partial x_k}\right\rangle - \langle u_k''\rangle\frac{\partial\langle p\rangle}{\partial x_k} + \langle u_i''\rangle\frac{\partial\langle\tau_{ik}\rangle}{\partial x_k} + \left\langle p'\frac{\partial u_k'}{\partial x_k}\right\rangle.\end{aligned} \tag{3.4}$$

The first term on the right-hand side of (3.4) represents the energy production; the second, turbulent diffusion; the third, diffusion resulting from velocity-pressure interaction; the fourth, viscous diffusion; the fifth, energy dissipation; and the last three are compressibility-related terms.

The mean kinetic energy and internal energy equations are

$$\begin{aligned}\frac{\partial \langle\rho\rangle\{u_k\}\{K\}}{\partial x_k} &= \langle\rho\rangle\{u_i''u_k''\}\frac{\partial\{u_i\}}{\partial x_k} - \frac{\partial\langle\rho\rangle\{u_k''K''\}}{\partial x_k} - \frac{\partial\langle p\rangle\langle u_k\rangle}{\partial x_k} \\ &\quad + \frac{\partial\langle\tau_{ik}\rangle\langle u_i\rangle}{\partial x_k} - \langle\tau_{ik}\rangle\frac{\partial\langle u_i\rangle}{\partial x_k} + \langle p\rangle\frac{\partial\langle u_k\rangle}{\partial x_k} + \langle u_k''\rangle\frac{\partial\langle p\rangle}{\partial x_k} - \langle u_i''\rangle\frac{\partial\langle\tau_{ik}\rangle}{\partial x_k}\end{aligned} \tag{3.5}$$

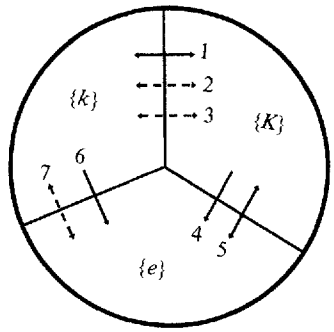

FIGURE 8. The energy transfer: 1. $\langle\rho\rangle\{u_i''u_k''\}\partial\{u_i\}/\partial x_k$, 2. $\langle u_k''\rangle\partial\langle p\rangle/\partial x_k$, 3. $\langle u_i''\rangle\partial\langle\tau_{ik}\rangle/\partial x_k$, 4. $\langle\tau_{ik}\rangle\partial\langle u_i\rangle/\partial x_k$ 5. $\langle p\rangle\partial\langle u_k\rangle/\partial x_k$, 6. $\langle\tau_{ik}'\partial u_i'/\partial x_k\rangle$ and 7. $\langle p'\partial u_k'/\partial x_k\rangle$. Terms 4 and 6 are irreversible and dashed arrows represent the additional compressibility terms due to turbulent density and pressure fluctuations.

and

$$\frac{\partial\langle\rho\rangle\{u_k\}\{e\}}{\partial x_k} = \langle\tau_{ik}\rangle\frac{\partial\langle u_i\rangle}{\partial x_k} + \left\langle\tau_{ik}'\frac{\partial u_i'}{\partial x_k}\right\rangle - \frac{\partial\langle\rho\rangle c_v\{u_k''T''\}}{\partial x_k} - \frac{\partial\langle q_k\rangle}{\partial x_k} - \langle p\rangle\frac{\partial\langle u_k\rangle}{\partial x_k} - \left\langle p'\frac{\partial u_k'}{\partial x_k}\right\rangle. \tag{3.6}$$

Figure 8 symbolizes energy transfer mechanisms among the internal energy, the mean and turbulent kinetic energies. Terms 2, 3 and 7 are the additional compressibility terms resulting from turbulent fluctuation: the first two, $\langle u_k''\rangle\partial\langle p\rangle/\partial x_k$ and $\langle u_i''\rangle\partial\langle\tau_{ik}\rangle/\partial x_k$, are responsible for the energy exchange between the mean and turbulent kinetic energies (cf. (3.5) and (3.4)) and the last (the pressure–dilatation correlation), $\langle p'\partial u_k'/\partial x_k\rangle$, accounts for an additional exchange between the internal and turbulent kinetic energies (cf. (3.6) and (3.4)).

It should be mentioned that the energy exchange shown in figure 8 is not unique. The classical diagram of Favre (1969) (see Lele 1994) shows that the interaction between $\{K\}$ and $\{T\}$ occurs via $\langle p\rangle\partial\{u_k\}/\partial x_k$ and $\langle\tau_{ik}\rangle\partial\{u_i\}/\partial x_k$ while here $\langle p\rangle\partial\langle u_k\rangle/\partial x_k$ and $\langle\tau_{ik}\rangle\partial\langle u_i\rangle/\partial x_k$ are responsible. This difference causes $\langle u_k''\rangle\partial\langle p\rangle/\partial x_k$ and $\langle u_i''\rangle\partial\langle\tau_{ik}\rangle/\partial x_k$ to appear as an exchange between $\{T\}$ and $\{k\}$ in the previous approach, while here it appears as an exchange between $\{K\}$ and $\{k\}$. We prefer to use the present representation rather than that of Favre because we believe that the Favre decomposition should only be applied in the convective terms and in the rest of the terms the Reynolds decomposition should be used, as mentioned above.

The term $\langle\tau_{ik}'\partial u_i'/\partial x_k\rangle$ in (3.4) and (3.6) is the energy dissipation rate per unit volume. For convenience, we use ϵ to denote this quantity throughout this paper. It should be distinguished from the conventional use of ϵ to represent the energy dissipation rate *per unit mass*. The difference is a factor of mean density, $\langle\rho\rangle$. Sarkar *et al.* (1989) and Zeman (1990) have proposed separating ϵ into solenoidal and dilatational parts: $\epsilon_s \equiv \langle\mu\rangle\langle\omega_i'\omega_i'\rangle$ (where ω_i' is the vorticity fluctuation) and $\epsilon_d \equiv 4/3\,\langle\mu\rangle\langle(\partial u_k'/\partial x_k)^2\rangle$, respectively. Strictly speaking, this splitting is valid only in *homogenous* flows (see Huang 1995). Moreover, as will be seen in §4.4, we find that for the flow under investigation the ratio of the (homogenous) dilatational dissipation to its solenoidal counterpart is so small that one can neglect the former. And since dilatational dissipation is small not only compared to the incompressible

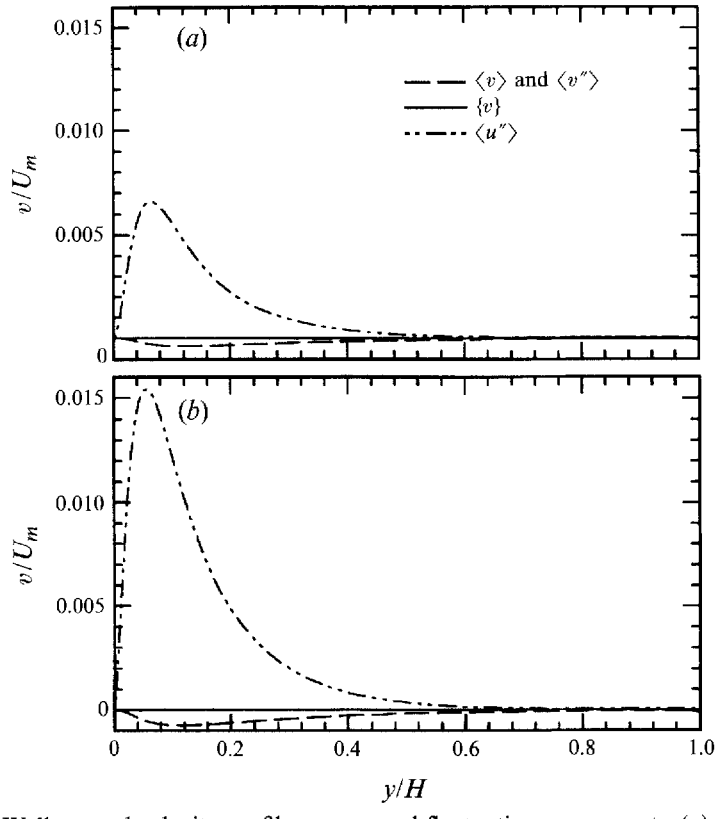

FIGURE 9. Wall-normal velocity profiles: mean and fluctuating components. (*a*) Case A, (*b*) Case B.

terms but also in comparison to other compressible terms, it appears unlikely that the dilational–solenoidal splitting is useful for the flow under investigation.

In a fully developed channel flow, the continuity equation leads to $\{v\} = 0$, which also implies $\langle v\rangle = \langle v''\rangle$. As shown in figure 9, the DNS results satisfy $\{v\} \approx 0$ and $\langle v\rangle \approx \langle v''\rangle$. However, even though $\langle v''\rangle$ (or $\langle v\rangle$) is much smaller than $\langle u''\rangle$, it is not zero. For the channel flow, for example, the conventional Reynolds-averaging decomposition leads to governing equations with a non-zero convective term while this term is absent from the equations using the Favre decomposition. This is one of the main attractions of the Favre decomposition.

In the DNS, the flow is driven by an external body force in order to avoid non-zero streamwise gradients of mean density and pressure, $\partial\langle\rho\rangle/\partial x$ and $\partial\langle p\rangle/\partial x$. Since it is in practice more relevant to explain the physics of a fully developed flow in terms of a pressure-driven one, an 'effective-pressure gradient' is introduced to relate the two flows. The body force f_i and effective-pressure gradient are essentially interchangeable in the momentum equation via

$$-\left(\frac{\partial p}{\partial x_i}\right)_{eff} = \rho f_i. \tag{3.7}$$

Since in the DNS f_i is assumed to be uniform in space, maintaining a prescribed value of mass flux $\dot{m} = \int_0^H \langle\rho u\rangle \mathrm{d}y/H = \int_0^H \langle\rho\rangle\{u\}\mathrm{d}y/H$, the mean effective-pressure

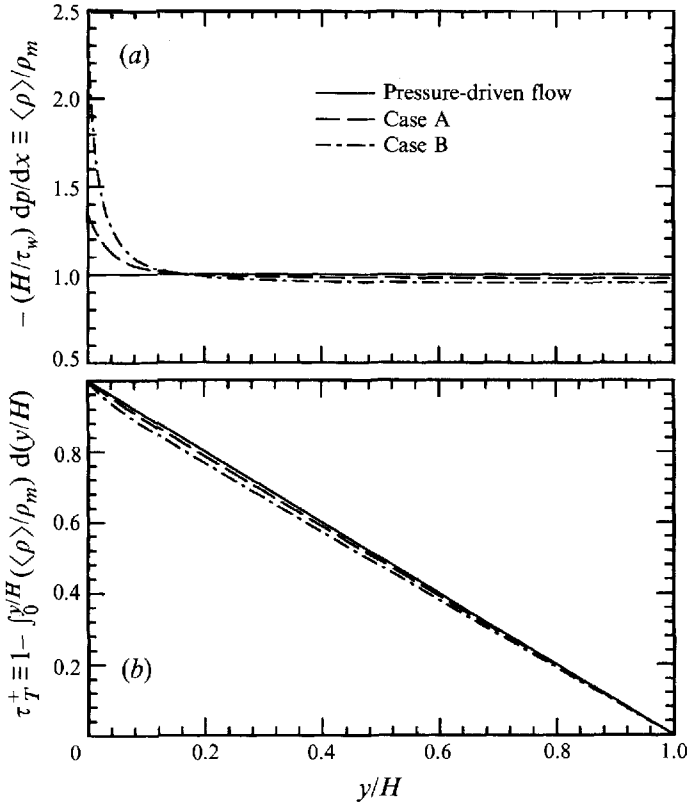

FIGURE 10. Pressure-driven *vs.* body-force-driven fully developed compressible turbulent channel flow. (*a*) Pressure gradient, (*b*) total shear stress.

gradient is a function of y:

$$\left(\frac{\partial\langle p\rangle}{\partial x}\right)_{eff} = -\frac{\tau_w}{H}\frac{\langle\rho\rangle}{\rho_m}. \tag{3.8}$$

Note however that because the body force is non-zero only in the streamwise momentum equation, this y-variation does not imply a non-zero wall-normal effective-pressure gradient, or artificially constrain the actual mean thermodynamic pressure, whose wall-normal gradient remains neglible (see Coleman *et al.* 1995). But there is a subtle difference between this body-force-driven fully developed channel flow and an actual pressure-driven fully developed channel flow, in which $\partial\langle p\rangle/\partial x = -\tau_w/H$ and the total shear stress varies linearly from the wall to the centre of the channel, $\langle\tau_T^+\rangle = 1 - y/H$ (besides the fact that $\partial\langle p\rangle/\partial x = 0$ in one but not the other). For the present body-force-driven flow, the momentum equation, when normalized by τ_w ($\equiv \rho_w u_\tau^2$), is

$$\langle\tau_T^+\rangle = \langle\tau_{12}{}^+\rangle - \frac{\langle\rho\rangle\{u''v''\}}{\rho_w u_\tau^2} = 1 - \frac{1}{H}\int_0^y \frac{\langle\rho\rangle}{\rho_m}\mathrm{d}y \tag{3.9}$$

where

$$\langle\tau_{12}{}^+\rangle = \frac{\langle\tau_{12}\rangle}{\tau_w} = \frac{\langle\mu\rangle}{\mu_w}\frac{\partial\langle u\rangle^+}{\partial y^+} + \left\langle\frac{\mu'}{\mu_w}\frac{\partial u^{+\prime}}{\partial y^+}\right\rangle. \tag{3.10}$$

Figure 10 is a comparison of the present and 'real' pressure-driven flows: figure 10(*a*) shows the dimensionless effective-pressure gradient, $-(H/\tau_w)(\partial\langle p\rangle/\partial x)_{eff} \equiv \langle\rho\rangle/\rho_m$,

and figure 10(*b*) the dimensionless total shear stress, $\langle\tau_T^+\rangle \equiv 1 - \int_0^y (\langle\rho\rangle/\rho_m)\mathrm{d}y/H$. As can be seen, although the variation of the effective-pressure gradient is noticeable, the overall effect on the total shear stress is fairly small. Thus, the differences between the body-force-driven flow and pressure-driven flows are too small to affect our conclusions.

In the DNS, the molecular viscosity is assumed to be a function of temperature according to $\mu/\mu_w = (T/T_w)^{0.7}$. Because $\langle T^{0.7}\rangle = \{T\}^{0.7}(1 + 0.7\langle T''\rangle/\{T\} - 0.105\langle T''^2\rangle/\{T\}^2 + O[\langle T''^3\rangle/\{T\}^3])$ and $\{T\} \gg \langle T''\rangle$, it follows that $\langle\mu\rangle/\mu_w = (\{T\}/T_w)^{0.7}$ is a good approximation in evaluating the Reynolds-averaged viscosity.

Note that the velocities in (3.10) are Reynolds, not Favre, averaged. As discussed in the previous section, this inconsistency exists in the molecular diffusion terms of all the transport equations and one could replace the Reynolds-averaged quantities with Favre-averaged variables using relationships derived in the previous section, such as (2.2), (2.12) and (2.13). Ristorcelli (1993) observed that $\langle v''\rangle$ is almost as large as $\langle v\rangle$ in a Mach 4.5 transitional boundary layer DNS (see Dinavahi & Pruett 1993) and argued that accurate accounting of the mass flux terms, $\langle u_i''\rangle$, is important in near-wall modelling. But since the v-momentum equation does not appear explicitly in the boundary-layer formulation, this problem may not be serious. For the present DNS, $\langle u\rangle \gg \langle u''\rangle$ (see figure 3), so the assumption that $\langle u\rangle \approx \{u\}$ is probably adequate. Indeed, replacing the Reynolds-averaged quantities in all of the viscous diffusion terms by the Favre-averaged quantities seems to be appropriate, because, as will be shown later, the assumption that $\langle f\rangle \gg \langle f''\rangle$ is valid in all equations governing the boundary-layer flow. On the other hand, this approximation may lead to a small error in evaluating the wall shear stress (or heat flux), since gradients are more sensitive to changes of the dependent variable. By substituting $\partial\langle u\rangle/\partial y = \partial\{u\}/\partial y + \partial\langle u''\rangle/\partial y$ into (3.10), one can write

$$\frac{\langle\mu\rangle}{\mu_w}\frac{\partial\{u\}^+}{\partial y^+} + \frac{\langle\mu\rangle}{\mu_w}\frac{\partial\langle u''\rangle^+}{\partial y^+} + \left\langle\frac{\mu'}{\mu_w}\frac{\partial u^{+\prime}}{\partial y^+}\right\rangle - \frac{\langle\rho\rangle\{u''v''\}}{\rho_w u_\tau^2} = 1 - \frac{1}{H}\int_0^y \frac{\langle\rho\rangle}{\rho_m}\mathrm{d}y. \tag{3.11}$$

Figure 11 shows profiles of all shear stress components in (3.11); for ease of reference, some material is repeated from figure 5. Also, the total shear stress in figure 11 is obtained by summing the left-hand side of (3.11), and may be compared with the results shown in figure 10, which are obtained from the right-hand side of (3.11) directly. For $y/H < 0.1$ ($y^* < 17$ approximately), the first term on the left-hand side of (3.11), the Favre-averaged viscous stress, dominates, and the maximum contributions from the second and the third terms are about 4% and 2% of the *total* stress close to the wall (Case B). For $y/H > 0.2$ ($y^* > 30$), the turbulent stress dominates and the overall behaviour is similar to that found for the incompressible DNS of Mansour *et al.* (1988).

Next we turn our attention to (3.3), the total energy equation. Since the 'fully developed' condition imposed in the DNS assumes that the temperature profile does not change in the streamwise direction, i.e. $\partial T/\partial x = 0$, an overall energy balance requires that the heat transfer into the walls equal the total pressure work done (or, the total heat generation) across the channel; i.e.

$$\begin{aligned} q_w &= \int_0^H \{u\}\left(\frac{\partial\langle p\rangle}{\partial x}\right)_{eff}\mathrm{d}y = -\frac{\tau_w}{H\rho_m}\int_0^H \langle\rho\rangle\{u\}\mathrm{d}y \\ &= -\frac{\tau_w}{H\rho_m}\int_0^H \langle\rho u\rangle\mathrm{d}y = -\frac{\tau_w\dot{m}}{\rho_m} = -\tau_w U_m. \end{aligned} \tag{3.12}$$

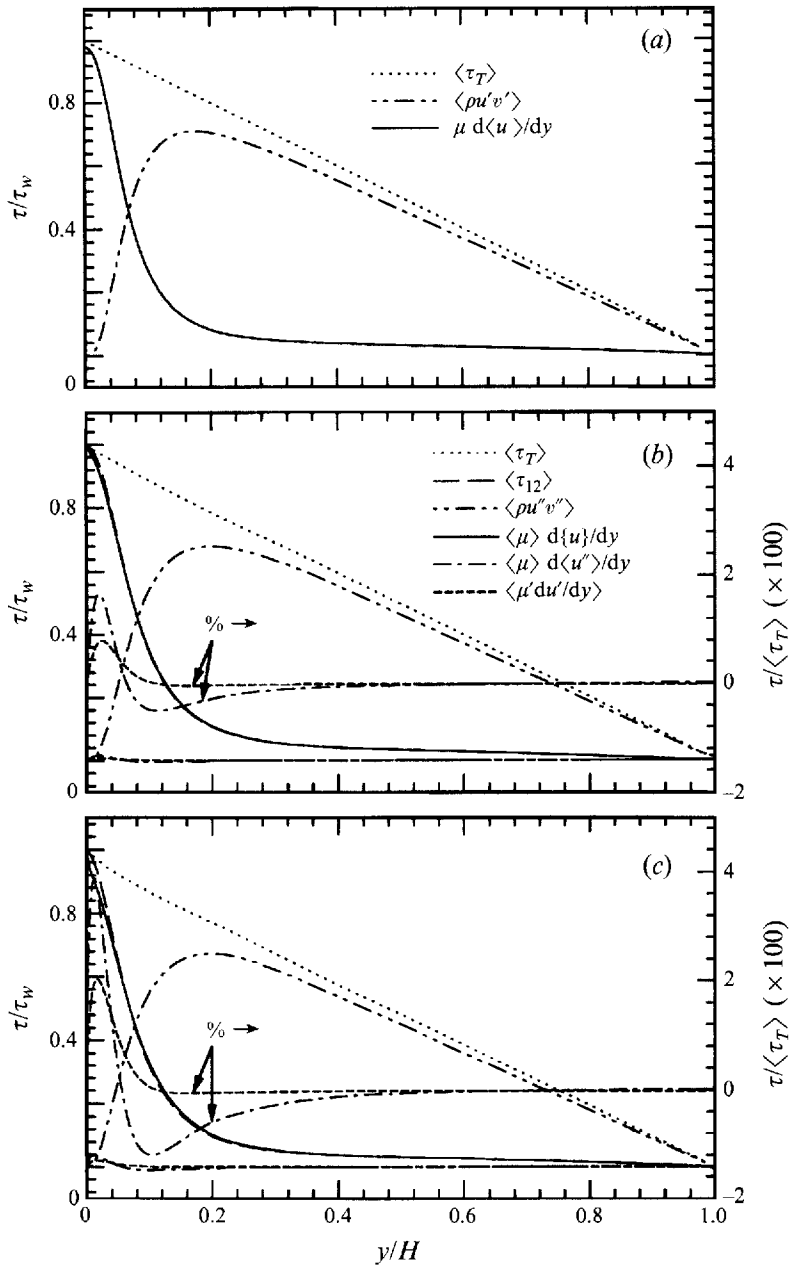

FIGURE 11. Decomposition of the shear stresses. Symbol τ denotes any contribution to shear stress. (*a*) Incompressible DNS (Mansour *et al.*), (*b*) Case A, (*c*) Case B.

The total energy equation is thus

$$-\left(\langle\tau_{i2}\rangle\langle u_i\rangle + \langle\tau_{i2}'u_i'\rangle - \langle q_2\rangle - \langle\rho\rangle\{v''K''\} - \langle\rho\rangle\{v''k''\} - \langle\rho\rangle c_p\{v''T''\}\right)$$
$$= q_w + \frac{\tau_w}{H\rho_m}\int_0^y \langle\rho\rangle\{u\}\mathrm{d}y, \qquad (3.13)$$

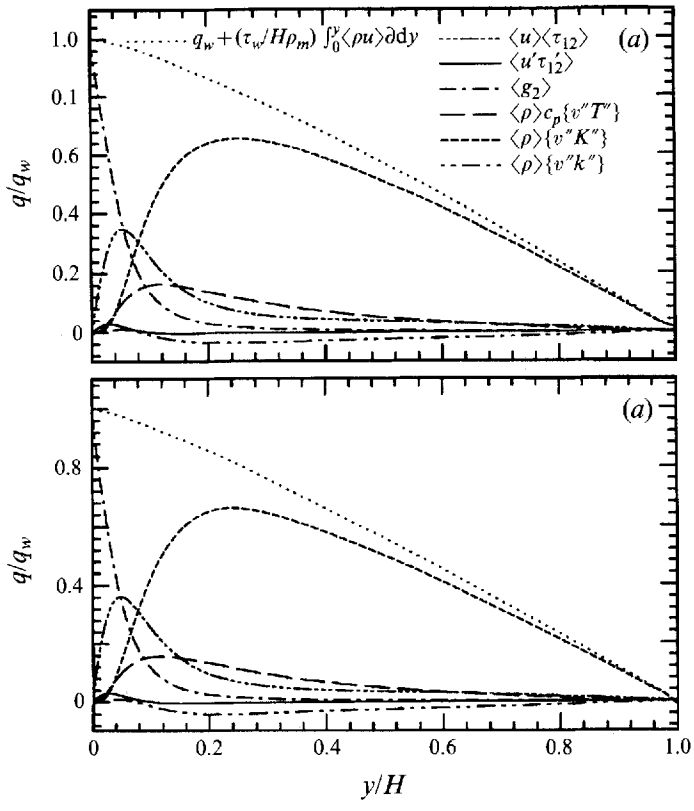

FIGURE 12. Decomposition of the heat fluxes. Symbol q denotes any contribution to heat flux. (*a*) Case A, (*b*) Case B.

where

$$\langle\tau_{i2}\rangle\langle u_i\rangle \approx \langle\mu\rangle\langle u_i\rangle\frac{\partial\langle u_i\rangle}{\partial y} + \langle u_i\rangle\left\langle\mu'\frac{\partial u_i'}{\partial y}\right\rangle$$
$$\approx \langle\mu\rangle\frac{\partial\langle K\rangle}{\partial y} + \left\langle\mu'\frac{\partial K'}{\partial y}\right\rangle - \langle u'\mu'\rangle\frac{\partial\langle u\rangle}{\partial y} \tag{3.14}$$

is the molecular diffusion of mean kinetic energy,

$$\langle\tau_{i2}'u_i'\rangle \approx \langle\mu\rangle\left\langle u_i'\frac{\partial u_i'}{\partial y}\right\rangle + \langle u_i'\mu'\rangle\frac{\partial\langle u_i\rangle}{\partial y} + \left\langle u_i'\mu'\frac{\partial u_i'}{\partial y}\right\rangle$$
$$\approx \langle\mu\rangle\frac{\partial\langle k\rangle}{\partial y} + \left\langle\mu'\frac{\partial k'}{\partial y}\right\rangle + \langle u'\mu'\rangle\frac{\partial\langle u\rangle}{\partial y} \tag{3.15}$$

is the molecular diffusion of turbulent kinetic energy, and

$$\langle q_2\rangle = -\langle\alpha\rangle\frac{\partial\langle T\rangle}{\partial y} - \left\langle\alpha'\frac{\partial T'}{\partial y}\right\rangle \tag{3.16}$$

is the molecular diffusion of the internal energy. For simplicity, some insignificant terms have been omitted from (3.14) and (3.15) (see Huang 1995 for a detailed discussion). Figure 12 shows the contributions of all the energy fluxes that appear in (3.13). Although the values of Mach number and wall temperature for Cases A and B are different, their total energy budgets, when normalized by the heat flux at the wall, are nearly the same.

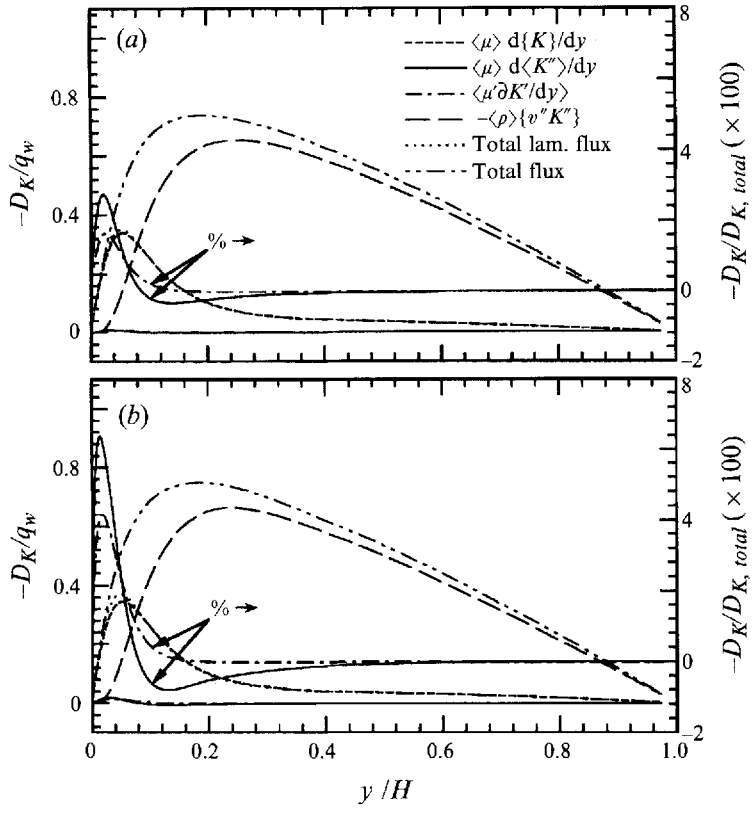

FIGURE 13. Diffusion of mean kinetic energy, K. Symbol D_K denotes any contribution to diffusion of $\{K\}$. (*a*) Case A, (*b*) Case B.

By substituting (3.14), (3.15) and (3.16) into (3.13), the latter becomes

$$-\left(\langle\mu\rangle\frac{\partial\langle K\rangle}{\partial y}+\left\langle\mu'\frac{\partial K'}{\partial y}\right\rangle+\langle\mu\rangle\frac{\partial\langle k\rangle}{\partial y}+\left\langle\mu'\frac{\partial k'}{\partial y}\right\rangle+\langle\alpha\rangle\frac{\partial\langle T\rangle}{\partial y}+\left\langle\alpha'\frac{\partial T'}{\partial y}\right\rangle\right.$$
$$\left.-\langle\rho\rangle\{u\}\{u''v''\}-\tfrac{1}{2}\langle\rho\rangle\{v''u_i''u_i''\}-\langle\rho\rangle c_p\{v''T''\}\right)$$
$$=q_w+\frac{\tau_w}{H\rho_m}\int_0^y\langle\rho\rangle\{u\}\mathrm{d}y. \tag{3.17}$$

Furthermore, by replacing the Reynolds-averaged variables in the molecular diffusion by Favre-averaged quantities, the total energy equation for fully developed channel flow can be expressed as

$$-\left(\langle\mu\rangle\frac{\partial\{K\}}{\partial y}+\langle\mu\rangle\frac{\partial\langle K''\rangle}{\partial y}+\left\langle\mu'\frac{\partial K'}{\partial y}\right\rangle\right.$$
$$+\langle\mu\rangle\frac{\partial\{k\}}{\partial y}+\langle\mu\rangle\frac{\partial\langle k''\rangle}{\partial y}+\left\langle\mu'\frac{\partial k'}{\partial y}\right\rangle+\langle\alpha\rangle\frac{\partial\{T\}}{\partial y}+\langle\alpha\rangle\frac{\partial\langle T''\rangle}{\partial y}+\left\langle\alpha'\frac{\partial T'}{\partial y}\right\rangle$$
$$\left.-\langle\rho\rangle\{u\}\{u''v''\}-\tfrac{1}{2}\langle\rho\rangle\{v''u_i''u_i''\}-\langle\rho\rangle c_p\{v''T''\}\right)=q_w+\frac{\tau_w}{H\rho_m}\int_0^y\langle\rho\rangle\{u\}\mathrm{d}y, \tag{3.18}$$

where the first to third, the fourth to sixth and the seventh to ninth terms on the left-hand side of (3.18) represent the molecular diffusion of $\{K\}$, $\{k\}$ and $\{T\}$, respectively.

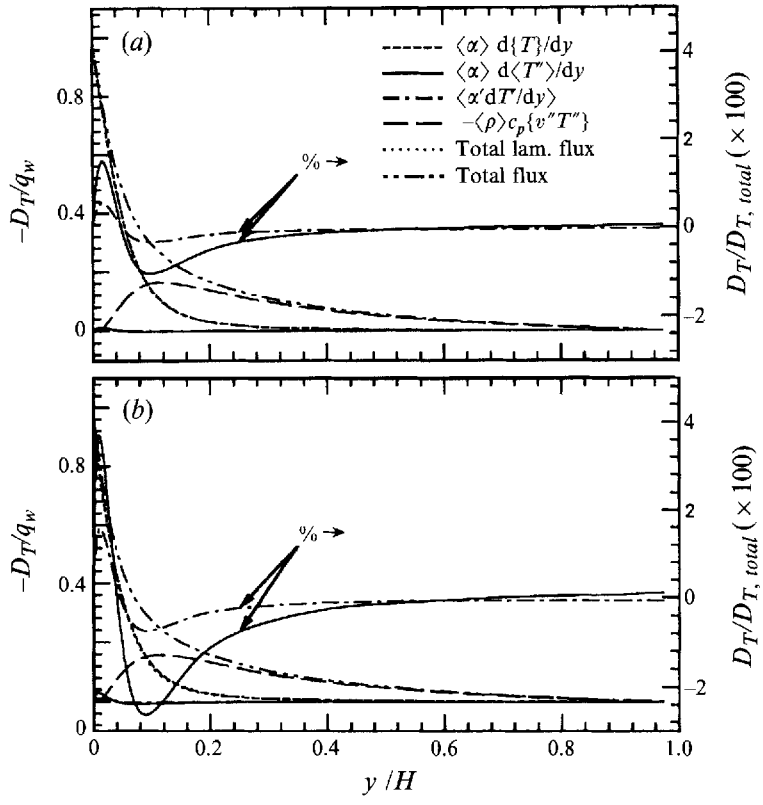

FIGURE 14. Diffusion of internal energy, T. Symbol D_T denotes any contribution to diffusion of $\{T\}$. (*a*) Case A, (*b*) Case B.

The last three terms (the tenth to twelfth) are the corresponding contributions to turbulent diffusion. Figures 13, 14 and 15 show all diffusive components of $\{K\}$, $\{T\}$ and $\{k\}$, respectively. As can be seen from the figures, the diffusive transports of $\{K\}$ and $\{T\}$ are the dominant contributions and are at least one order of magnitude larger than diffusive transport of $\{k\}$. Moreover, for the viscous diffusion, contributions due to turbulent fluctuations and μ'-correlations are small compared to the corresponding primary Favre viscous diffusion, $\langle\mu\rangle\partial\{f\}/\partial y$, where $f \equiv K, k$ or T.

For a fully developed channel flow the turbulent kinetic energy equation, (3.4), reduces to

$$-\frac{\partial}{\partial y}\left(\langle\tau_{12}'u'\rangle - \tfrac{1}{2}\langle\rho\rangle\{v''u_i''u_i''\} - \langle p'v'\rangle\right)$$
$$= -\langle\rho\rangle\{u''v''\}\frac{\partial\{u\}}{\partial y} - \epsilon - \langle v''\rangle\frac{\partial\langle p\rangle}{\partial y} + \langle u''\rangle\frac{\partial\langle\tau_{12}\rangle}{\partial y} + \phi_{ii}, \qquad (3.19)$$

where $\phi_{ii} \equiv \langle p'\partial u_k'/\partial x_k\rangle$. Figure 16(*a–c*) shows budgets of the turbulent kinetic energy for the incompressible DNS of Mansour *et al.* and Cases A and B of the compressible DNS, respectively. The incompressible and compressible data sets were both normalized by $\tau_w U_m/H$. The reason for using this mixture of inner and outer variables is that, as equation (3.12) shows for the present flow, $\tau_w U_m/H$ is equal to $-q_w/H$, while figure 12 shows that the individual heat fluxes for $\{K\}$, $\{k\}$ and $\{e\}$ are almost independent of Mach number and wall temperature when normalized by

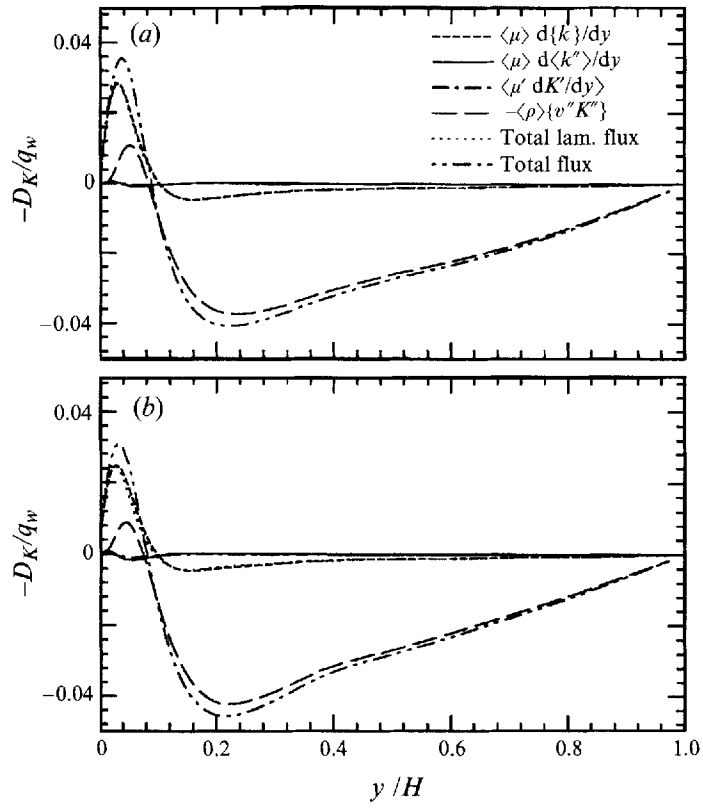

FIGURE 15. Diffusion of turbulent kinetic energy, k. Symbol D_k denotes any contribution to diffusion of $\{k\}$. (*a*) Case A, (*b*) Case B.

q_w. Normalization by $\tau_w U_m/H$ therefore seems the best choice for the present cases, but is not suggested as the optimum for general spatially developing flows. As can be seen from figures 16(*b*) and 16(*c*), the normalized budgets for all three DNS cases are very similar; also, the collective compressibility contribution (i.e. the sum of the last three terms on the right-hand side of (3.19)), is found to be negligible. The individual compressibility contributions are plotted separately in figure 17. As can be seen, they are limited to $y/H < 0.2$ (more generally $y^* < 30$) since the major compressibility contribution comes from $\langle u''\rangle \partial\langle\tau_{12}\rangle/\partial y$, in which both $\langle u''\rangle$ and $\langle\tau_{12}\rangle$ are significant only in the viscous region. This term is negative and therefore transfers turbulent kinetic energy back to the mean flow. A detailed discussion on relations between viscous diffusion and dissipation appears in Huang (1995).

By substituting (2.13) and (3.15) into (3.19), the equation for turbulent kinetic energy in fully developed compressible channel flow becomes

$$-\frac{\partial}{\partial y}\left(\langle\mu\rangle\frac{\partial\{k\}}{\partial y}+\langle\mu\rangle\frac{\partial\langle k''\rangle}{\partial y}+\left\langle\mu'\frac{\partial k'}{\partial y}\right\rangle-\langle\mu\rangle\frac{\partial\tfrac{1}{2}\langle u_i''\rangle^2}{\partial y}+\langle\mu' u'\rangle\frac{\partial\langle u\rangle}{\partial y}\right.$$
$$\left.-\tfrac{1}{2}\langle\rho\rangle\{v''u_i''u_i''\}-\langle p'v'\rangle\right)=-\langle\rho\rangle\{u''v''\}\frac{\partial\{u\}}{\partial y}-\epsilon-\langle v''\rangle\frac{\partial\langle p\rangle}{\partial y}+\langle u''\rangle\frac{\partial\langle\tau_{12}\rangle}{\partial y}+\phi_{ii}. \tag{3.20}$$

The molecular diffusion of turbulent kinetic energy consists of five contributions, indicated by the first five terms on the left-hand side of (3.20). The first three terms,

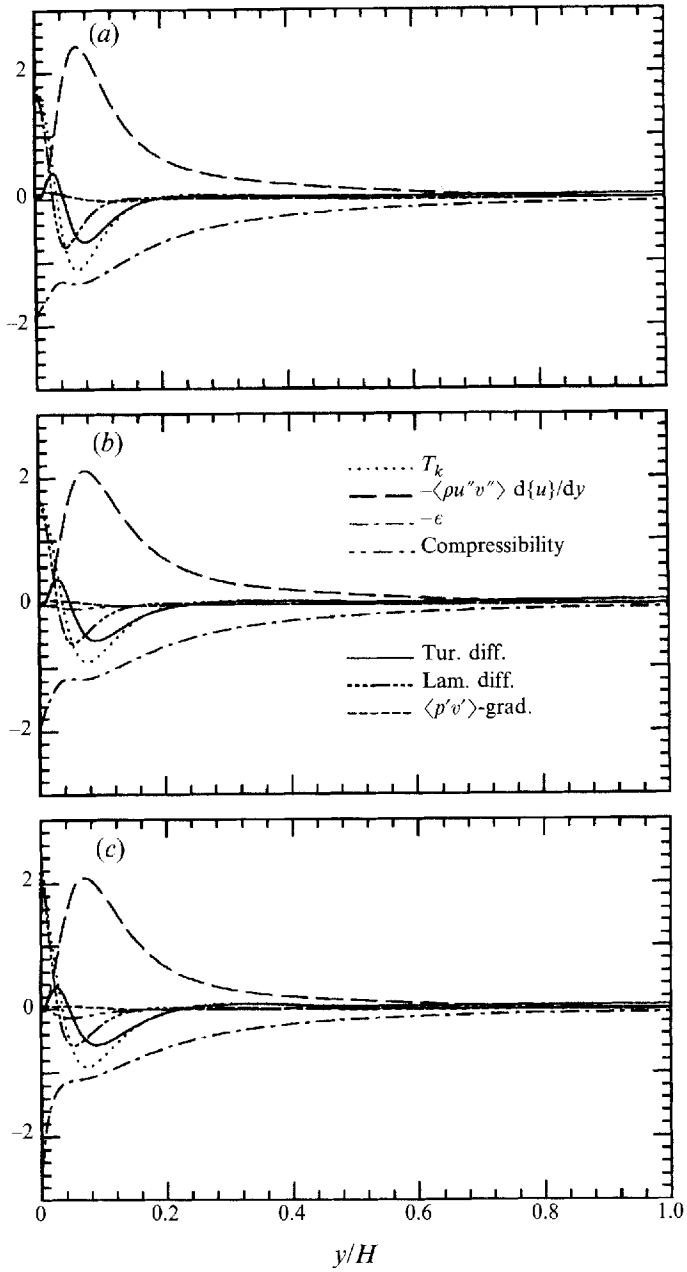

FIGURE 16. Turbulent energy budgets. Symbol T_k denotes the transport contribution of $\{k\}$. (*a*) Incompressible DNS (Mansour *et al.*), (*b*) Case A, (*c*) Case B.

representing the molecular diffusion due to the Favre-averaged mean component, the mean Favre-fluctuating component, and the correlation between viscosity fluctuation and fluctuating-turbulent-energy gradient, respectively, are similar to the molecular diffusion terms in the mean-flow equations. The fourth and fifth terms (not appearing in the molecular diffusion terms in the total kinetic energy equation) are responsible for the additional energy exchange between the turbulent kinetic energy and the mean

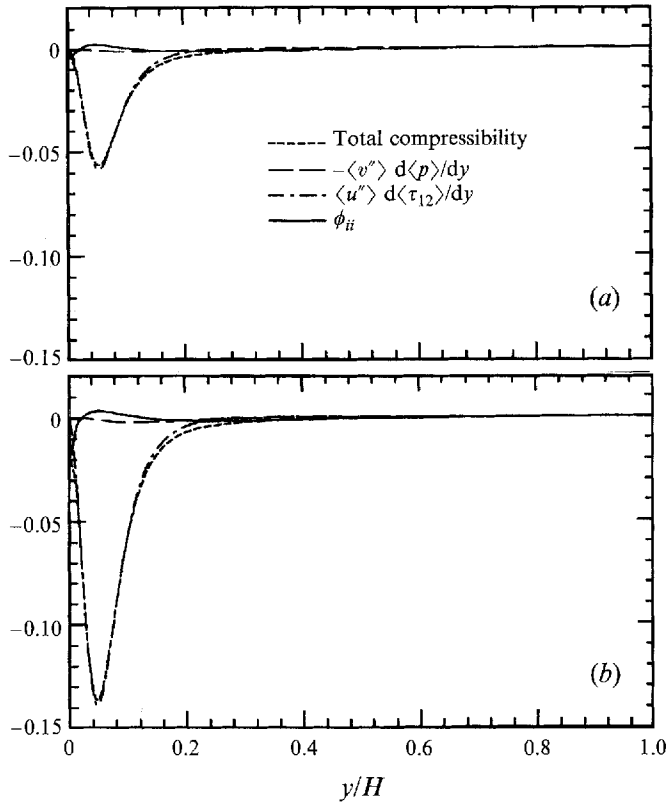

FIGURE 17. Compressibility contributions. (*a*) Case A, (*b*) Case B.

kinetic energy, since these terms also appear, with opposite sign, at the end of the first line of the mean kinetic energy equation:

$$-\frac{\partial}{\partial y}\left(\langle\mu\rangle\frac{\partial\{K\}}{\partial y}+\langle\mu\rangle\frac{\partial\langle K''\rangle}{\partial y}+\left\langle\mu'\frac{\partial K'}{\partial y}\right\rangle+\langle\mu\rangle\frac{\partial\frac{1}{2}\langle u_i''\rangle^2}{\partial y}-\langle\mu' u'\rangle\frac{\partial\langle u\rangle}{\partial y}\right.$$
$$\left.-\langle\rho\rangle\{u\}\{u''v''\}-\langle p\rangle\langle v\rangle\right)=\langle\rho\rangle\{u''v''\}\frac{\partial\{u\}}{\partial y}-\langle\tau_{12}\rangle\frac{\partial\langle u\rangle}{\partial y}+\langle p\rangle\frac{\partial\langle v\rangle}{\partial y}$$
$$+\langle v''\rangle\frac{\partial\langle p\rangle}{\partial y}-\langle u''\rangle\frac{\partial\langle\tau_{12}\rangle}{\partial y}-\{u\}\frac{\partial\langle p\rangle}{\partial x}. \tag{3.21}$$

Figure 18 presents a comparison of all the components of the molecular diffusion. Results are plotted only for the near-wall region ($y/H < 0.3$) since the molecular diffusion is important only here. As the figure shows, the major contribution comes from the diffusion of Favre-averaged turbulent kinetic energy. An interesting observation is that $\partial(\langle\mu' u'\rangle\partial\langle u\rangle/\partial y)/\partial y$ is the second largest term while $\partial/\partial y\,[\langle\mu\rangle\partial(\langle u_i''\rangle^2/2)/\partial y]$ is negligible. Very close to the surface ($y/H < 0.04$, $y^* < 8$), the former diffusive term represents a gain of turbulent kinetic energy from the mean kinetic energy while in the outer part of the buffer layer (up to $y/H \approx 0.15$, $y^* \approx 24$) the same amount of energy is transferred back to the mean kinetic energy by the same mechanism, owing to the integral of this term across the channel being zero.

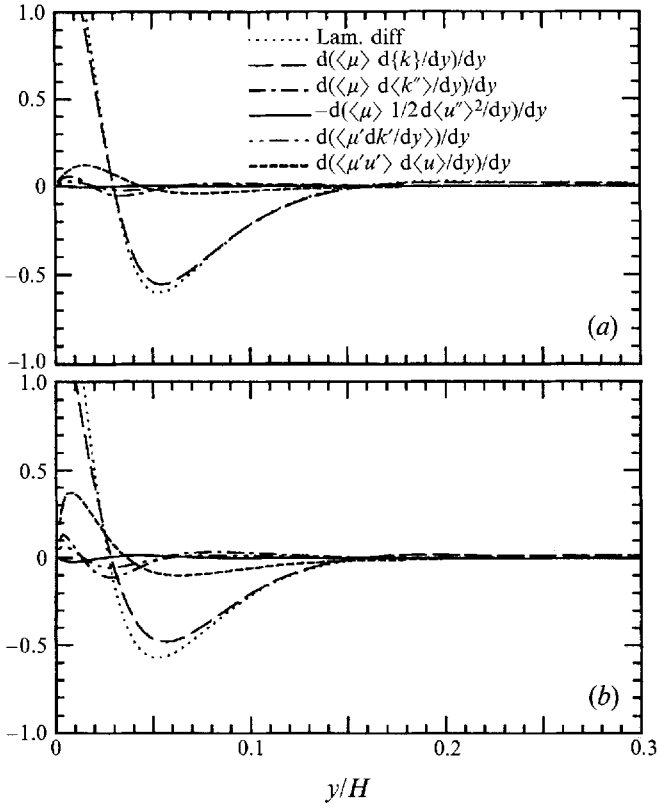

FIGURE 18. Decomposition of molecular diffusion of turbulent kinetic energy, k. (*a*) Case A, (*b*) Case B.

4. Modeling issues

4.1. *On the strong Reynolds analogy*

The strong Reynolds analogy (SRA) suggested by Morkovin (1964) is based on the assumption that the fluctuation in total temperature is nearly zero, so that $c_p T' + K' + k' = 0$. By assuming that $K' \gg k'$, and also that the two-dimensional boundary-layer approximation applies so that $\langle u\rangle u' \gg \langle v\rangle v'$ and $\langle w\rangle w'$, the following relation can be obtained:

$$\frac{T'/\langle T\rangle}{(\gamma-1)M^2u'/\langle u\rangle} \approx -1. \tag{4.1}$$

To take heat flux at the wall into account, Cebeci & Smith (1974) employed a similarity relation between u and T, namely $(T_T - T_w)/(T_{T,o} - T_w) = u/u_o$ (where subscripts o and T indicate the free-stream (or centreline) value and the total quantity, respectively), to derive an extended form of strong Reynolds analogy (ESRA):

$$\frac{T'/\langle T\rangle}{(\gamma-1)M^2u'/\langle u\rangle} \approx -\left[1 + \frac{c_p(\langle T_w\rangle - \langle T_{T,o}\rangle)}{\langle u\rangle\langle u_o\rangle}\right]. \tag{4.2}$$

Although the SRA agrees well with measurements for boundary layers over adiabatic walls, Gaviglio (1987) reported that neither the SRA nor ESRA is adequate for non-adiabatic flows. Gaviglio (1987) and Rubesin (1990) have independently derived

a relationship between u' and T' as follows:

$$\frac{T'/\langle T\rangle}{(\gamma-1)M^2u'/\langle u\rangle} \approx \frac{1}{c\left(\partial\langle T_T\rangle/\partial\langle T\rangle - 1\right)}. \tag{4.3}$$

Gaviglio chose $c = 1$ and Rubesin $c = 1.34$. They both reported good agreement with measurements. We now show that c is approximately equal to the turbulent Prandtl number, $Pr_t = (\{u''v''\}\partial\{T\}/\partial y)/(\{v''T''\}\partial\{u\}/\partial y)$. The factor c arises from 'mixing length' relations,

$$u' \propto \frac{\partial\langle u\rangle}{\partial y}, \tag{4.4}$$

$$T' \propto \frac{\partial\langle T\rangle}{\partial y}, \tag{4.5}$$

which can be combined to give

$$u'\frac{\partial\langle T\rangle}{\partial y} = cT'\frac{\partial\langle u\rangle}{\partial y}. \tag{4.6}$$

This can be viewed as a *definition* of c. Making the key assumption that c is independent of time, and multiplying (4.6) by $\rho v'$ and averaging both sides, yields

$$\langle\rho u'v'\rangle\frac{\partial\langle T\rangle}{\partial y} = c\langle\rho v'T'\rangle\frac{\partial\langle u\rangle}{\partial y}. \tag{4.7}$$

By substituting (2.5) and (2.6) into (4.7) and assuming $\langle u\rangle = \{u\}$ and $\langle T\rangle = \{T\}$, one can show that

$$c = \frac{\langle\rho u'v'\rangle\partial\langle T\rangle/\partial y}{\langle\rho v'T'\rangle\partial\langle u\rangle/\partial y} \approx \frac{\{v''u''\}\partial\{T\}/\partial y}{\{v''T''\}\partial\{u\}/\partial y} = Pr_t. \tag{4.8}$$

Finally, (4.6) can thus be written as

$$\frac{T'/\langle T\rangle}{(\gamma-1)M^2u'/\langle u\rangle} \approx \frac{1}{Pr_t}\frac{\partial\langle T\rangle}{\partial\langle u\rangle}\frac{c_p}{\langle u\rangle} \approx \frac{\{v''T''\}}{\{u''v''\}}\frac{c_p}{\langle u\rangle}. \tag{4.9}$$

Applying $\partial\langle u\rangle/\partial\langle T\rangle \approx (\partial\langle T_T\rangle/\partial\langle T\rangle - 1)c_p/\langle u\rangle$ in (4.9), the following can be derived:

$$\frac{T'/\langle T\rangle}{(\gamma-1)M^2u'/\langle u\rangle} \approx \frac{1}{Pr_t}\frac{1}{\left(\partial\langle T_T\rangle/\partial\langle T\rangle - 1\right)}. \tag{4.10}$$

The coefficient of correlation between u' and T' is numerically about 0.8–0.9 (and negative in boundary layers on not-too-cold walls) whereas (4.10) implies a correlation coefficient of unity. We therefore expect that if (4.10) is used to evaluate other velocity–temperature statistics, errors on at least the 20% level will occur even if c is replaced by Pr_t. Nevertheless (4.10) is an improvement over (4.2) for first estimates.

Figure 19(*a*) shows the variation of the dimensionless total temperature fluctuations, $\langle T_T'^2\rangle^{1/2}/T_w$, across the channel. As can be seen, the total-temperature fluctuation is not negligible in the present very-cold-wall DNS. Profiles of the turbulent Prandtl number across the channel are presented in figure 19(*b*). They are close to the incompressible DNS results of Kim & Moin (1989) everywhere except for $0.1 < y/H < 0.3$ – the buffer region – where the compressible DNS results display a rapid increase of mean temperature (figure 4). The high temperature in this region increases the molecular viscosity and hence the thickness of the buffer zone. As a result, the Prandtl-number plateau is slightly closer to the centreline than in the

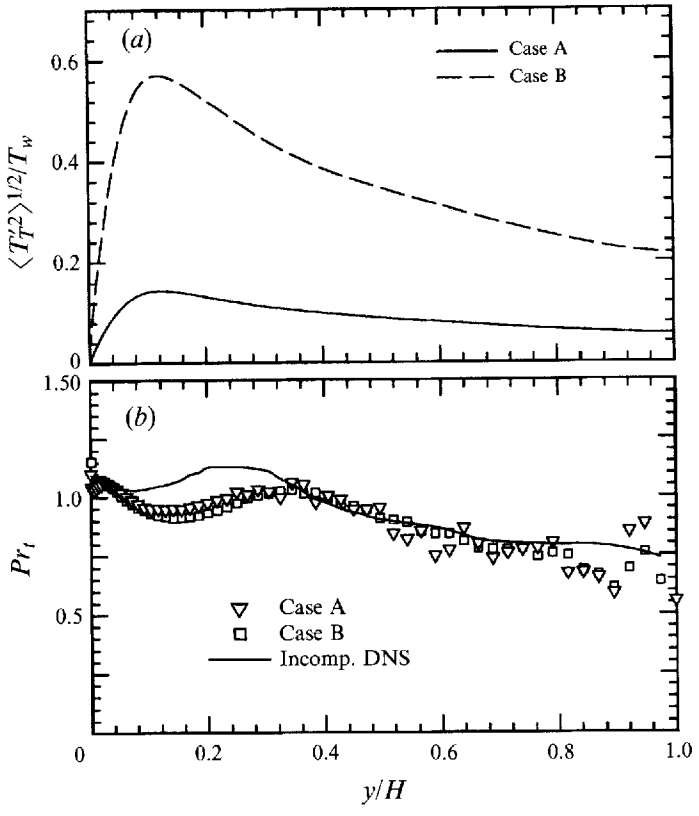

FIGURE 19. Profiles of (*a*) total temperature fluctuations and (*b*) turbulent Prandtl number.

incompressible DNS. The Prandtl number peaks at approximately $y^* = 40$, 50 and 50 for the incompressible DNS and Cases A and B, respectively. The turbulent Prandtl number drops with increasing y after the plateau and the profiles agree very well with the incompressible results. The fluctuations found for $y/H > 0.3$ in the compressible cases are caused by both $\partial\{u\}/\partial y$ and $\{v''T''\}$ in the definition of Pr_t approaching zero towards the centreline. The asymptotic-wall Prandtl number is about 1.1 for both Mach numbers. This is in accordance with the incompressible DNS.

Comparisons of the ESRA and (4.10) (or (4.9)) for the two cases are presented in figure 20. It is found that the ESRA experiences a change of sign near $y/H = 0.2$ (note that results in figure 20 are in terms of root mean squares, $\langle u'^2\rangle^{1/2}$ and $\langle T'^2\rangle^{1/2}$). The DNS data show a drop of $(\langle T'^2\rangle^{1/2}/\langle T\rangle)/\left[(\gamma-1)M^2\langle u'^2\rangle^{1/2}/\langle u\rangle\right]$ towards the channel centre but the ESRA predicts a rise. In contrast, (4.10) mimics the DNS trends fairly well, particularly in the viscous region. Gaviglio's and Rubesin's analogies, which in effect assume $Pr_t = 1$ and 1.34, respectively, display trends similar to (4.10), although they predict somewhat lower values of $(\langle T'^2\rangle^{1/2}/\langle T\rangle)/\left[(\gamma-1)M^2\langle u'^2\rangle^{1/2}/\langle u\rangle\right]$ near $y/H = 1$.

4.2. *On modelling the mean Favre-averaged fluctuations,* $\langle f''\rangle$

To evaluate the mean Favre-averaged fluctuations, such as $\langle u_i''\rangle$ and $\langle T''\rangle$, we have followed the approach of Rubesin (1990) by assuming that the fluid behaves in a

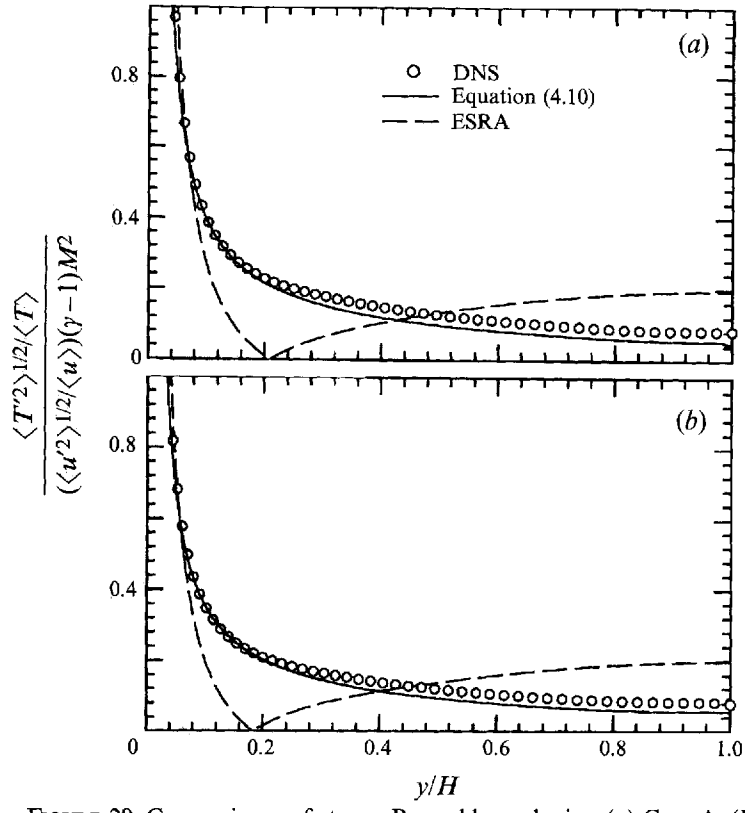

FIGURE 20. Comparisons of strong Reynolds analogies: (*a*) Case A, (*b*) Case B.

polytropic manner:

$$\frac{p'}{\langle p\rangle} = n\frac{\rho'}{\langle\rho\rangle} = \frac{n}{n-1}\frac{\rho T'}{\langle\rho\rangle\langle T\rangle}, \tag{4.11}$$

where the polytropic coefficient, n, becomes a turbulence model parameter. By substituting (4.9) into (4.11), one finds

$$\frac{\rho'}{\langle\rho\rangle} \approx \frac{1}{n-1}\frac{1}{\langle T\rangle}\frac{\{v''T''\}}{\{u''v''\}}\frac{\rho u'}{\langle\rho\rangle} \approx \frac{1}{n-1}\frac{1}{\{T\}}\frac{\{v''T''\}}{\{u''v''\}}\frac{\rho u'}{\langle\rho\rangle}. \tag{4.12}$$

Hence, for any variable $\langle f''\rangle$, one can obtain:

$$\begin{aligned}\langle f''\rangle &= -\frac{\langle\rho' f''\rangle}{\langle\rho\rangle} \approx -\frac{1}{n-1}\frac{1}{\{T\}}\frac{\{v''T''\}}{\{u''v''\}}\frac{\langle\rho u' f''\rangle}{\langle\rho\rangle} \\ &= -\frac{1}{n-1}\frac{1}{\{T\}}\frac{\{v''T''\}}{\{u''v''\}}\frac{\langle\rho u'' f''\rangle}{\langle\rho\rangle} = -\frac{1}{n-1}\frac{1}{\{T\}}\frac{\{v''T''\}}{\{u''v''\}}\{u''f''\}.\end{aligned} \tag{4.13}$$

Figure 21 shows comparisons of $\langle u''\rangle$, $\langle v''\rangle$ and $\langle T''\rangle$ with (4.13) using $n = 0$, corresponding to an isobaric process (implying negligible p'; see figure 14 of Coleman *et al.* 1995). As can been seen from the figure, the agreement is very good.

We also examined the $\langle u_i''\rangle$-model proposed by Rubesin (1990)

$$\langle u_i''\rangle = -c_{\langle u_i''\rangle}\frac{\{k\}}{\epsilon}\{u_i''u_j''\}\frac{\partial\{T\}}{\partial x_j}\frac{1}{\{T\}}. \tag{4.14}$$

This model is similar to the one used by Zeman (1993), who, using the boundary-layer

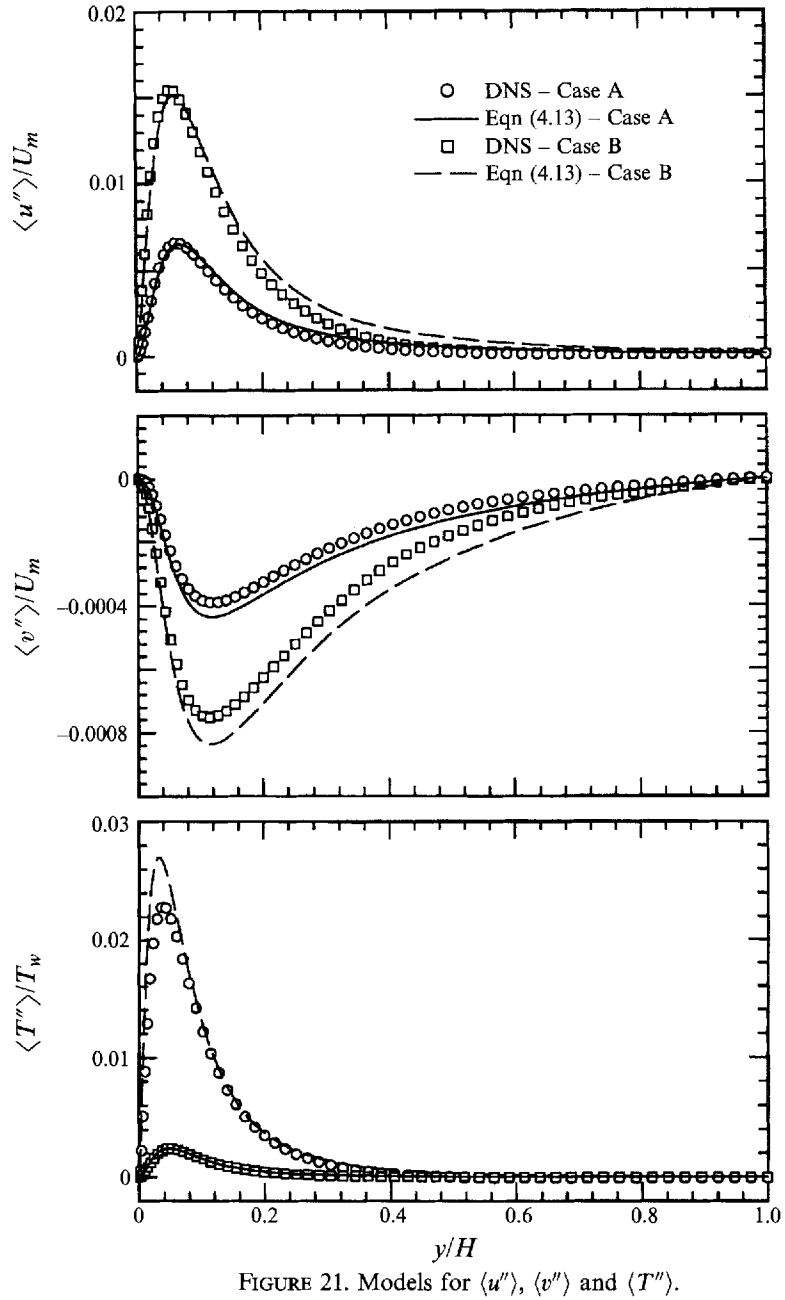

FIGURE 21. Models for $\langle u'' \rangle$, $\langle v'' \rangle$ and $\langle T'' \rangle$.

approximation $\partial\langle p \rangle/\partial y = 0$, replaced $\partial\{T\}/\{T\}$ by $-\partial\langle \rho \rangle/\langle \rho \rangle$. Unfortunately, no unique value of $c_{\langle u_i'' \rangle}$ can be found to satisfy equations for $\langle u'' \rangle$ and $\langle v'' \rangle$ simultaneously. To match the DNS data, it was found that $c_{\langle u'' \rangle}$ and $c_{\langle v'' \rangle}$ should be 1.1 and 0.21, respectively, which implies that (4.14) is a less general model than (4.13).

4.3. *On modelling the pressure–dilatation term,* $\phi_{ii} \equiv \langle p' \partial u_k'/\partial x_k \rangle$

Based on the observation of figures 16 and 17, we conclude that the contribution of the pressure–dilatation term to the turbulent kinetic energy budget is negligible.

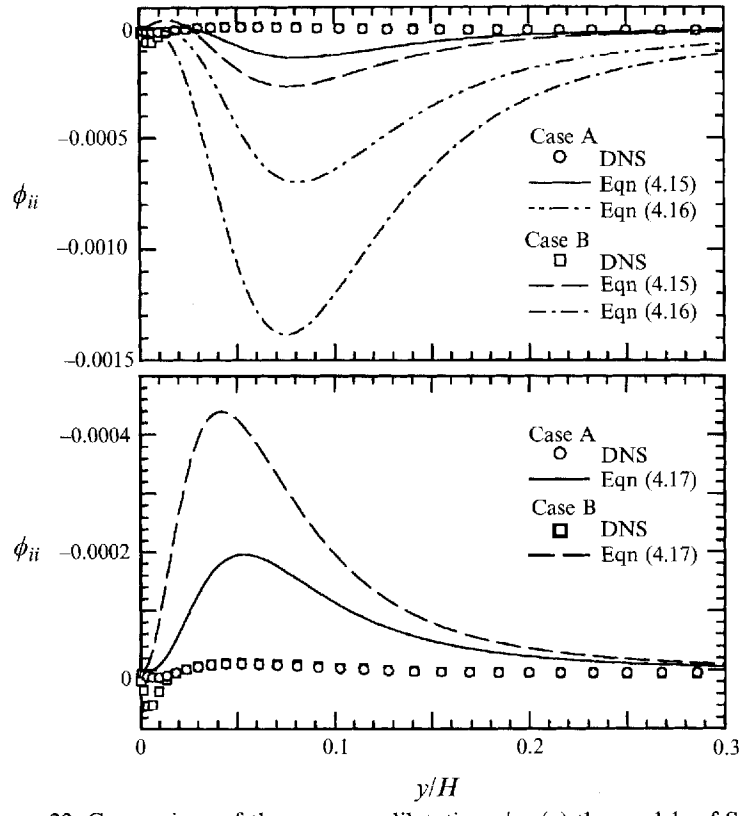

FIGURE 22. Comparison of the pressure–dilatation, ϕ_{ii}: (*a*) the models of Sarkar *et al.*, and el Baz and Launder models, and (*b*) Rubesin's model with $n = 1$.

Hence, any realistic model should predict that this term is insignificant when applied to the supersonic flows under consideration.

Sarkar, Erlebacher & Hussaini (1992) proposed that the pressure–dilatation term could be related to the turbulent Mach number, M_t, the turbulent energy generation, $P_k \equiv -\{u_i''u_k''\}\partial\{u_i\}/\partial x_k$, and the solenoidal part of the dissipation rate, ϵ_s, according to

$$\phi_{ii} = -0.8\langle\rho\rangle P_k M_t^2 + 0.4\langle\rho\rangle\epsilon_s M_t^2 \tag{4.15}$$

where the coefficients are two times larger than those reported by Sarkar *et al.* (1992) because they use $M_t \equiv (2\langle k\rangle)^{1/2}/\langle a\rangle$ to define the turbulent Mach number.

El Baz & Launder (1993) proposed

$$\phi_{ii} = 3\langle\rho\rangle\left(\frac{4}{3}\{k\}\frac{\partial\{u_i\}}{\partial x_i} - P_k\right)M_t^2. \tag{4.16}$$

Unfortunately, as can be seen from figure 22(*a*), these models not only produce a negative ϕ_{ii} throughout the channel but also unrealistically overestimate its magnitude. They were designed mainly to decrease turbulent kinetic energy as Mach number increases in order to mimic the behaviour of compressible mixing layers, and evidently are unsuitable for wall flows as they stand.

Rubesin (1990) made use of a $\langle p'^2\rangle$ equation to deduce the pressure–dilatation term, which appears as a source (or sink) in that equation. First, a $\langle\rho'^2\rangle$ equation is derived from the continuity equation for the fluctuating density. To obtain the

$\langle p'^2 \rangle$ equation, Rubesin assumed a polytropic process, (4.11), to replace ρ' with p'. A similar approach has also been adopted by Zeman (1993), who assumed an isentropic process ($n = \gamma$). If transport terms are negligible, the $\langle \rho'^2 \rangle$ equation reduces to a equation for the pressure–dilatation term:

$$\phi_{ii} = n\langle p \rangle \frac{\langle u_i'' \rangle}{\langle \rho \rangle} \frac{\partial \langle \rho \rangle}{\partial x_i}. \tag{4.17}$$

Rubesin and Zeman derived their closures for ϕ_{ii} by substituting their models of the $\langle u_i'' \rangle$ equations, (4.14), into (4.17). In this discussion, we shall restrict our attention to the original form of the ϕ_{ii} model, (4.17), since the $\langle u_i'' \rangle$ are directly available from the DNS data.

Figure 22(*b*) compares (4.17) and the DNS data. The ϕ_{ii} values are normalized by $\rho_m U_m^3/H$. Since ϕ_{ii} is significant only close to the wall, results are shown only for $0 < y/H < 0.3$. For purpose of comparison, we have chosen $n = 1$ in (4.17). As can be seen from the figure, the DNS results indicate that ϕ_{ii} drops below zero in the region very close to the wall ($y/H < 0.02$, $y^* < 5$) and Case B displays a larger dip than Case A. The values of ϕ_{ii} are positive in the region $0.02 < y/H < 0.12$ and negative for $y/H > 0.12$. The two DNS profiles resemble each other, except in the negative region very close to the wall. In contrast, the ϕ_{ii} obtained from the polytropic relation (4.17) remains positive throughout the channel and is about one order of magnitude larger than the DNS results. Moreover, in contrast to the DNS results, the profiles of the two cases predicted by (4.17) are different, the magnitude in Case B being larger than in Case A.

Zeman (1993) used $n = \gamma = 1.4$ in (4.17). In addition, he proposed multiplying the right-hand side of (4.17) by a function that depends on M_t: $0.02(1 - \exp(-M_t^2/0.2))$ (We were informed by the late Dr Zeman that this expression is misprinted in Zeman 1993). Since the magnitude of M_t in Case B is again larger than that in Case A (figure 1), the discrepancy between the two profiles becomes even more pronounced if Zeman's functional factor is included.

Huang, Bradshaw & Coakley (1994) have shown that the conventional $k-\epsilon$ model fails when applied to compressible boundary layers. They concluded that the model coefficients must be functions of mean density gradients if the unmodified $k-\epsilon$ model is to successfully predict the compressible (Van Driest) law of the wall, for example. A different viewpoint, however, was raised by Huang (1991) and later by Zeman (1993). They demonstrated that the modelled form of ϕ_{ii} shown in (4.17) can remedy the problem in the $k-\epsilon$ model. This remedy implies that the failure of the $k-\epsilon$ model was due to compressibility effects – specifically, it was argued that the lack of the pressure–dilatation term was the cause of the problem. Since the degree of density dependence for model coefficients may vary from model to model (see Huang *et al.* 1994), but ϕ_{ii} is virtually unaffected by the choice of the model, apparently ϕ_{ii} is not the cause of the problem. We believe that by showing that the compressibility effects are small, the current study provides a clear-cut answer: the $k-\epsilon$ model (and any other model using the ϵ-equation) fails because the ϵ-equation contains extra (unphysical) terms when transformed to the compressible regime (a detailed discussion is given by Huang *et al.* 1994). Hence, the approach of Huang (1991) or Zeman (1993) should be considered only as an unphysical 'quick fix' to the $k-\epsilon$ model. For supersonic boundary layers we instead recommend a more rational and physical choice: simply setting $n = 0$ in (4.17) (again, assuming an isobaric process) and neglecting the pressure–dilatation term entirely.

4.4. *On the dilatational turbulent dissipation*

Another interesting development in the modelling of compressible turbulence is the concept of dilatational dissipation. In homogeneous compressible turbulent flows with constant viscosity, the turbulent energy dissipation can be cast into the sum of only two components – the solenoidal and dilatational parts. Otherwise, the turbulent energy dissipation consists of more than these two components. Substituting (2.21) into the definition for the turbulent energy dissipation, $\langle \tau_{ik}' \partial u_i'/\partial x_k \rangle$, yields

$$\epsilon \equiv \left\langle \tau_{ik}' \frac{\partial u_i'}{\partial x_k} \right\rangle = \epsilon_1 + \epsilon_2 + \epsilon_3, \tag{4.18}$$

where

$$\epsilon_1 = \langle \mu \rangle \left\langle \frac{\partial u_i'}{\partial x_k} \left(\frac{\partial u_i'}{\partial x_k} + \frac{\partial u_k'}{\partial x_i} \right) \right\rangle - \frac{2}{3} \langle \mu \rangle \left\langle \frac{\partial u_i'}{\partial x_k} \frac{\partial u_l'}{\partial x_l} \right\rangle \delta_{ik}, \tag{4.19}$$

$$\epsilon_2 = \left\langle \mu' \frac{\partial u_i'}{\partial x_k} \left(\frac{\partial u_i'}{\partial x_k} + \frac{\partial u_k'}{\partial x_i} \right) \right\rangle - \frac{2}{3} \left\langle \mu' \frac{\partial u_i'}{\partial x_k} \frac{\partial u_l'}{\partial x_l} \right\rangle \delta_{ik}, \tag{4.20}$$

$$\epsilon_3 = \left\langle \mu' \frac{\partial u_i'}{\partial x_k} \right\rangle \left(\frac{\partial \langle u_i \rangle}{\partial x_k} + \frac{\partial \langle u_k \rangle}{\partial x_i} \right) - \frac{2}{3} \left\langle \mu' \frac{\partial u_i'}{\partial x_k} \right\rangle \frac{\partial \langle u_l \rangle}{\partial x_l} \delta_{ik}. \tag{4.21}$$

The quantity ϵ_1 can be expressed as the sum of three parts: the solenoidal and dilatational contributions to dissipation, and an inhomogeneous term:

$$\epsilon_1 = \epsilon_s + \epsilon_d + \epsilon_I \tag{4.22}$$

where

$$\epsilon_s = 2\langle \mu \rangle \langle \omega_{ij}' \omega_{ij}' \rangle; \text{ with } \omega_{ij}' = \left(\frac{\partial u_i'}{\partial x_j} - \frac{\partial u_j'}{\partial x_i} \right) /2, \tag{4.23}$$

$$\epsilon_d = \frac{4}{3} \langle \mu \rangle \left\langle \frac{\partial u_l'}{\partial x_l} \frac{\partial u_k'}{\partial x_k} \right\rangle, \tag{4.24}$$

$$\epsilon_I = 2\langle \mu \rangle \left(\frac{\partial^2 \langle u_i' u_j' \rangle}{\partial x_i \partial x_j} - 2 \frac{\partial}{\partial x_i} \left\langle u_i' \frac{\partial u_j'}{\partial x_j} \right\rangle \right). \tag{4.25}$$

Figure 23 compares the ratio of ϵ_d to ϵ_s. It is very small throughout the channel – being less than 0.03% except in the region very close to the wall (the maximum value is about 0.1%, in Case B). This is in surprising contrast to DNS results for homogeneous shear flows (see Sarkar *et al.* 1992; Blaisdell, Mansour & Reynolds 1993), which show ratios of 10–20%. Moreover, when the ratio is plotted against turbulent Mach number, M_t, as shown in figure 23(*b*), the results for the two compressible channel cases are very different, indicating that ϵ_d/ϵ_s and M_t are not correlated. Again, this is in contrast to the observation of Blaisdell *et al.* (1993), who found that ϵ_d/ϵ_s is nearly proportional to M_t^2 in homogeneous shear flows.

Since the splitting of ϵ into solenoidal and dilatational dissipation is exact only in homogeneous flows with constant viscosity, the magnitudes of the inhomogeneous part, ϵ_I, and terms associated with viscosity-fluctuation correlations, ϵ_2 and ϵ_3, are also of interest. Figure 24 shows the ratio of the solenoidal to the total dissipation, ϵ_s/ϵ; also shown are the additional effect of Reynolds-averaged $\langle \mu' \partial u_i'/\partial x_k \rangle$ in $(\epsilon_s + \epsilon_3)/\epsilon$ and the ratio including the inhomogeneous terms, $(\epsilon_s + \epsilon_3 + \epsilon_I)/\epsilon$. If we neglect ϵ_d, the departure of the latter curve away from unity can be viewed as the contribution from ϵ_2. As figure 24 illustrates, both ϵ_2 and ϵ_3 are significant only very close to the wall ($y/H < 0.1$, $y^* < 17$). One surprising finding is that ϵ_3, which involves the product of

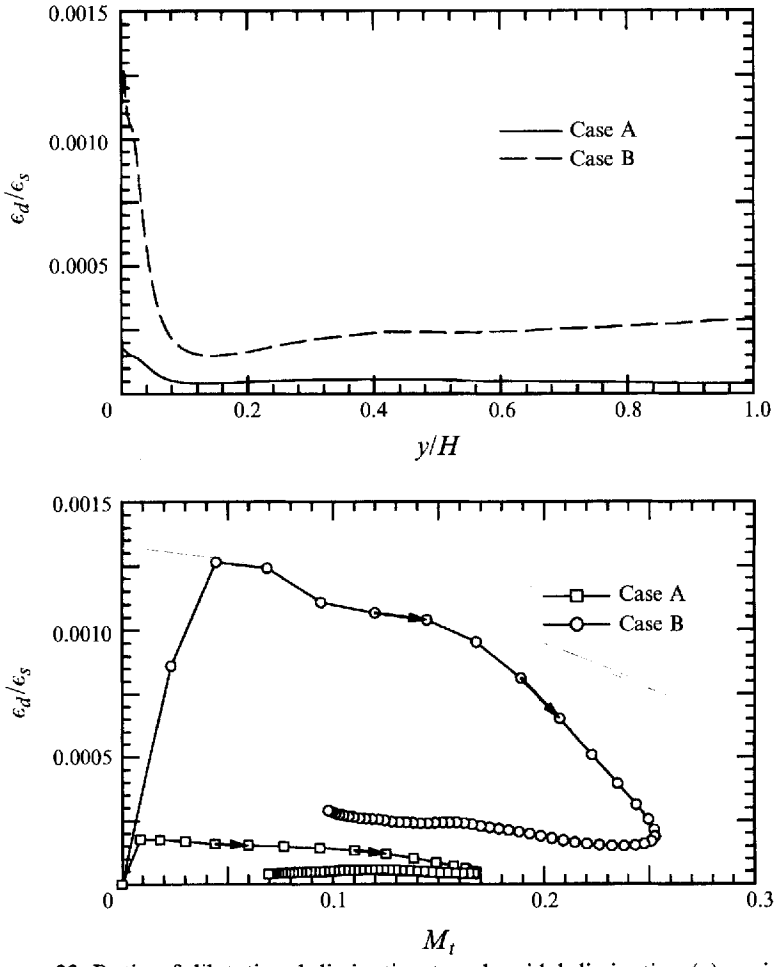

FIGURE 23. Ratio of dilatational dissipation to solenoidal dissipation (*a*) against y/H and (*b*) against turbulent Mach number, M_t. Arrows indicate direction of increasing y/H.

the correlation between the viscosity fluctuation and the velocity-gradient fluctuation, multiplied by the mean strain rate, is a significant fraction of the total dissipation in that region: maximum values are about 6% and 16% of the total for Cases A and B, respectively. Since $\mu' \propto T'$, and $T' \propto u'$ by (4.10), $\langle \mu' \partial u'/\partial y \rangle \propto \partial \langle u'^2 \rangle / \partial y$. Thus the major contribution to ϵ_3 in a thin shear layer, $\langle \mu' \partial u'/\partial y \rangle \partial \langle u \rangle / \partial y$, has a maximum deep in the viscous wall region and is much larger there than might be expected. Outside the viscous region both factors become small; according to our simplified analysis, ϵ_3 is zero in a homogeneous shear flow. On the other hand, ϵ_2 is small even in the viscous wall region, with maximum values about 1.5% and 2.5% of the total values for Cases A and B, respectively. The inhomogeneous contribution, ϵ_I, is nearly independent of Mach number and is about $\pm 3\%$ of the total value – this observation is in accordance with Bradshaw & Perot's (1993) investigation of incompressible DNS results. In incompressible flow, ϵ_I would be a pure transport term, integrating to zero over the flow volume: here it contains a source/sink part because the variable $\langle \mu \rangle$ is outside the derivative.

Finally, we note that ϵ_d and ϕ_{ii} are negligible not only for the isothermal-wall flow under investigation, but also for adiabatic flows at a higher Mach number: we have

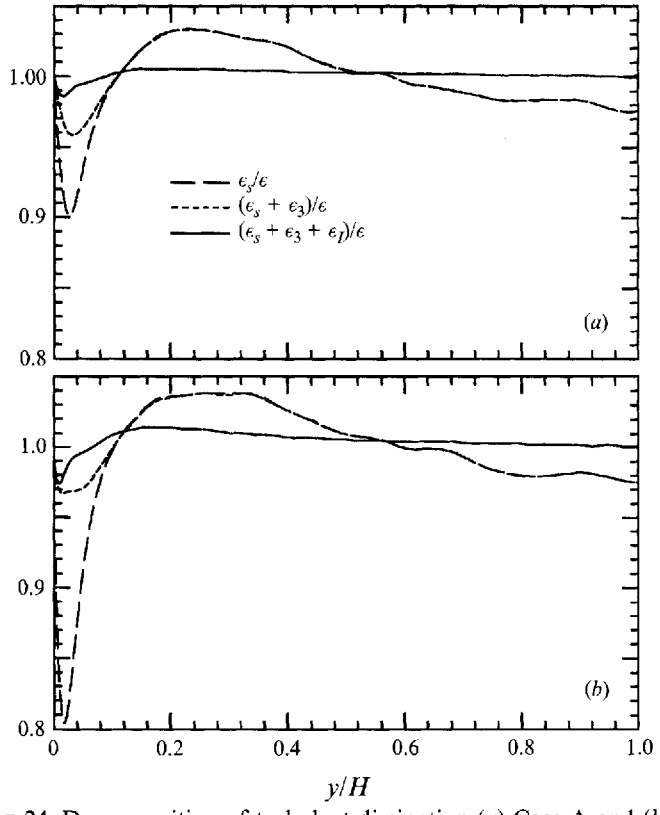

FIGURE 24. Decomposition of turbulent dissipation (*a*) Case A and (*b*) Case B.

been informed by Dr Yan Guo (private communication of work at DLR, Göttingen) that his direct numerical simulation of turbulent boundary layers on adiabatic walls at free-stream Mach numbers up to 6 also produces very small values for the dilatational dissipation and the pressure–dilatation correlation.

5. Conclusions

Analysis of DNS results has shown that for fully developed supersonic isothermal-wall channel flows:

(i) Differences between Reynolds (ensemble) averages and Favre averages for the streamwise velocity are small and are mainly observed in the region close to the surface.

(ii) For the shear stress and turbulent heat flux, $\langle \rho u'' v'' \rangle \approx \langle \rho u' v' \rangle$ and $\langle \rho v'' T'' \rangle \approx \langle \rho v' T' \rangle$ are adequate assumptions.

(iii) The DNS data confirm that when turbulent fluxes are scaled by the mean density variation, $\langle \rho \rangle / \rho_w$, the profiles collapse onto the corresponding incompressible curves.

(iv) The DNS results satisfy the mean momentum and energy equations very well. Contributions of the extra fluctuating diffusion rates, $\langle \mu \rangle \partial \langle f'' \rangle / \partial y$ and $\langle \mu' \partial f' / \partial y \rangle$, are found to be small and their influences limited to regions close to the surface.

(v) By isolating and studying in detail modes of energy exchange among internal, mean kinetic and turbulent kinetic energies, compressibility effects due to turbulent fluctuations are found to be unimportant.

(vi) The DNS results do not support previous forms of the strong Reynolds analogy for non-adiabatic flows. A more general representation of the analogy has been derived and shown to match the DNS results very well.

(vii) Equations for $\langle u'' \rangle$, $\langle v'' \rangle$ and $\langle T'' \rangle$, which have been derived using a new strong Reynolds analogy, agree very well with the DNS data.

(viii) Existing models for ϕ_{ii} and ϵ_d were all found to grossly overestimate these quantities in the present flows.

The support of NASA Ames Research Center (grant NCC2-452) for the first author, and the Stanford/NASA-Ames Center for Turbulence Research for the second, is appreciated. Partial support for the third author was provided by a Visiting Scientist appointment at the Research Institute for Advanced Computer Studies. Computer resources for the DNS work were provided by the NASA-Ames Advanced Computational Facility and the Numerical Aerodynamic Simulation project. Direct collaboration with the staff of the Modeling and Experimental Validation Branch at NASA-Ames has been stimulating, fruitful and pleasant.

REFERENCES

BAZ, A. M. EL & LAUNDER B. E. 1993 Second-moment modelling of compressible mixing layers. In *Engineering Turbulence Modelling and Experiments* (ed W. Rodi & F. Martelli). Elsevier.

BLAISDELL, G. A., MANSOUR, N. N. & REYNOLDS, W. C. 1993 Compressibility effects on the growth and structure of homogeneous turbulent shear flow. *J. Fluid Mech.* **256**, 443–485.

BRADSHAW, P. & PEROT, J. B. 1993 A note on turbulent energy dissipation in the viscous wall region. *Phys. Fluids* A **5**, 3305–3306.

CEBECI, T. & SMITH A. M. O. 1974 *Analysis of Turbulent Boundary Layers.* Academic Press.

COLEMAN, G. N., BUELL J. C., KIM, J. & MOSER, R. D. 1993 Direct simulation of compressible wall-bounded turbulence. In *9th Turbulent Shear Flows Conference, Aug. 16–18, Kyoto, Japan.*

COLEMAN, G. N., KIM, J. & MOSER, R. D. 1995 A numerical study of turbulent supersonic isothermal-wall channel flow. *J. Fluid Mech.* **305**, 159–183.

DINAVAHI, S. P. G. & PRUETT, C. D. 1993 Analysis of direct numerical simulation data of a Mach 4.5 transitional boundary layer flow. *ASME Fluids Engineering Conference, June 21–24, Washington DC.*

FAVRE, A. 1969 Statistical equations of turbulent gases. *Problems of Hydrodynamics and Continuum Mechanics*, pp. 231–266. Philadelphia: SIAM.

FERNHOLZ, H. H. & FINLEY, P. J. 1980 A critical commentary on mean flow data for two-dimensional compressible turbulent boundary layers. *AGARD-AG*-253.

GAVIGLIO, J. 1987 Reynolds analogies and experimental study of heat transfer in the supersonic boundary layer. *Intl J. Heat Mass Transfer* **30**, 911–926.

HUANG, P. G. 1991 Comment on the present statc and the future direction of second order closure models for compressible flows. *Workshop on Engineering Turbulence Modeling. NASA CP*-10088.

HUANG, P. G. 1995 Relations between viscous diffusion and dissipation of turbulent kinetic energy. Presented at the *Tenth Symposium on Turbulent Shear Flows, Penn. State U., Aug. 14–16,* pp. 2-79–2-84.

HUANG, P. G., BRADSHAW, P. & COAKLEY, T. J. 1993 Skin friction and velocity profile family for compressible turbulent boundary layers. *AIAA J.* **31**, 1600–1604.

HUANG, P. G., BRADSHAW, P. & COAKLEY, T. J. 1994 Turbulence models for compressible boundary layers. *AIAA J.* **32**, 735–740.

HUANG, P. G. & COLEMAN, G. N. 1994 Van Driest transformation and compressible wall-bounded flows. *AIAA J.* **32**, 2110–2113 (and Errata *AIAA J.* **33**, 1756).

KIM, J. & MOIN, P. 1989 Transport of passive scalars in a turbulent channel flow. In *Turbulent Shear Flows 6* (ed. J.-C. André *et al.*). Springer.

KIM, J., MOIN, P. & MOSER, R. D. 1987 Turbulence statistics in fully developed channel flow at low Reynolds number. *J. Fluid Mech.* **177**, 133–166.

LELE, S. K. 1994 Compressibility effects on turbulence. *Ann. Rev. Fluid Mech.* **26**, 211–254.

MANSOUR, N. N., KIM, J. & MOIN, P. 1988 Reynolds-stress and dissipation-rate budgets in a turbulent channel flow. *J. Fluid Mech.* **194**, 15–44.

MORKOVIN, M. V. 1964 Effects of compressibility on turbulent flows. In *Mechanique de la Turbulence* (ed. A. Favre), pp. 367–380. Gordon and Breach.

REYNOLDS, O. 1895 On the dynamical theory of incompressible viscous fluids and the determination of the criterion. *Phil. Trans. R. Soc. Lond.* A **186**, 123–164.

RISTORCELLI, J. R. 1993 A representation for the turbulent mass flux contribution to Reynolds-stress and two-equation closures for compressible turbulence. *ICASE Rep.* 93-88.

RUBESIN, M. W. 1990 Extra compressibility terms for Favre-averaged two-equation models of inhomogeneous turbulent flows. *NASA CR*-177556.

SARKAR, S. 1995 The stabilizing effect of compressibility in turbulent shear flow. *J. Fluid Mech.* **282**, 163–186.

SARKAR, S., ERLEBACHER, G. & HUSSAINI, M. Y. 1992 Compressible homogeneous shear: simulation and modeling. In *Turbulent Shear Flows 8* (ed. F. Durst *et al.*). Springer.

SARKAR, S., ERLEBACHER, G., HUSSAINI, M. Y. & KREISS, H. O. 1989 The analysis and modeling of dilatational terms in compressible turbulence. *J. Fluid Mech.* **227**, 473–493.

SPINA, E. F., SMITS, A. J. & ROBINSON, S. K. 1994 The physics of supersonic turbulent boundary layers. *Ann. Rev. Fluid Mech.* **26**, 287–319.

VAN DRIEST, E. R. 1951 Turbulent boundary layer in compressible fluids. *J. Aero. Sci.* **18**, 145–160 and 216.

ZEMAN, O. 1990 Dilatational dissipation: the concept and application in modeling compressible turbulence. *Phys. Fluids* A **2**, 178-188.

ZEMAN, O. 1993 New model for super/hypersonic turbulent boundary layers. *AIAA Paper* 93-0897.